

Effects of non-commutative geometry on black hole properties

A. A. Araújo Filho,^{1,*} J. R. Nascimento,^{1,†} A. Yu. Petrov,^{1,‡} P. J. Porfírio,^{1,§} and Ali Övgün^{2,¶}

¹*Departamento de Física, Universidade Federal da Paraíba, Caixa Postal 5008, 58051-970, João Pessoa, Paraíba, Brazil.*

²*Physics Department, Eastern Mediterranean University, Famagusta, 99628 North Cyprus, via Mersin 10, Turkiye*

(Dated: June 19, 2024)

In this study, we investigate the signatures of a non-commutative black hole solution. Initially, we calculate the thermodynamic properties of the system, including entropy, heat capacity, and Hawking radiation. For the latter quantity, we employ two distinct methods: surface gravity and the topological approach. Additionally, we examine the emission rate and remnant mass within this context. Remarkably, the lifetime of the black hole, after reaching its final state due to the evaporation process, is expressed analytically up to a *grey-body* factor. We estimate the lifetime for specific initial and final mass configurations. Also, we analyze the tensorial quasinormal modes using the 6th-order WKB method. Finally, we study the deflection angle, i.e., gravitational lensing, in both the weak and strong deflection limits.

Keywords: Black holes; Noncommutative geometry; Thermodynamics; Quasinormal modes; Gravitational lensing.

I. INTRODUCTION

In the domain of general relativity, the formalism used to depict spacetime geometry lacks a precise boundary on distance measurements, often regarding the Planck length as a foundational constraint. To address this challenge, scholars commonly explore the concept of non-commutative spacetimes. The motivation for exploring non-commutative geometry stems from its connections to string/M-theory [1–3], with notable applications observed in the domain of supersymmetric Yang-Mills theories, particularly within the superfield framework [4–6]. Additionally, the Seiberg-Witten map serves as a common tool for introducing non-commutativity into gravitational theories by gauging an appropriate group [7]. This framework has led to significant advancements in understanding black holes, encompassing their dynamics of evaporation [8, 9] and thermodynamic characteristics [10–14].

Nicolini et al. [15] introduced a significant discovery regarding the non-commutative effect. They proposed a novel model that alters the matter source term while preserving the Einstein tensor part of the field equation. In this model, the conventional point-like mass density on the Einstein equation is substituted by either a Gaussian smeared distribution or a Lorentzian distribution. These distributions are defined as $\rho_{\Theta} = M(4\pi\Theta)^{-\frac{3}{2}}e^{-\frac{r^2}{4\Theta}}$ and $\rho_{\Theta} = M\sqrt{\Theta}\pi^{-\frac{3}{2}}(r^2 + \pi\Theta)^{-2}$, respectively. A novel approach for incorporating non-commutativity into gravitational scenarios has emerged in the literature, fundamentally treating it as a perturbation [16].

Gravitational waves and their characteristics are crucial for understanding a diverse array of physical phenomena, ranging from early universe events to astrophysical occurrences such as stellar oscillations and binary systems [17–23]. These waves exhibit diverse intensities and modes, with their spectral attributes intricately linked to their sources [24]. Notably, the emission of gravitational waves from black holes holds significant importance. Following the collapse of matter, BHs emit radiation characterized by unique frequencies termed *quasinormal* modes [25–42]. In the literature, it is widely employed the weak field approximation method to study these modes within black hole contexts, encompassing general relativity and other gravitational theories, as well as scenarios involving Lorentz violation and related fields [43–72].

Recent advancements, particularly the detection of gravitational waves by the LIGO-Virgo collaboration [73–75], have expanded the scope of cosmological research. Gravitational waves are now used to explore the universe, including studying gravitational lensing within the weak field approximation [76–78]. Historically, gravitational lensing studies focused on light traveling great distances from the gravitational source, such as in Schwarzschild spacetime [79], and

*Electronic address: dilto@fisica.ufc.br

†Electronic address: jroberto@fisica.ufpb.br

‡Electronic address: petrov@fisica.ufpb.br

§Electronic address: pporfirio@fisica.ufpb.br

¶Electronic address: ali.ovgun@emu.edu.tr

were later extended to general spherically symmetric and static spacetimes [80]. However, in regions with strong gravitational fields, like those near black holes, the angular deviation of light is greatly amplified.

Observations from the Event Horizon Telescope of a supermassive black hole at the center of the M87 galaxy have generated significant scientific interest [62, 81–90]. Early work by Virbhadra and Ellis introduced a concise lens equation for supermassive black holes within an asymptotically flat background [91, 92], showing multiple symmetrically distributed images around the optic axis due to strong gravitational effects. Further advancements made by Frittelli et al. [93], Bozza et al. [94], and Tsukamoto [95] have enhanced the analytical frameworks for studying strong field gravitational lensing. These studies have examined light deflection in various contexts, including Reissner-Nordström spacetime [96–98], rotating solutions [99–104], exotic constructs like wormholes [105–109], and modified gravity theories [110].

In this study, we explore the characteristics of a non-commutative black hole solution. We begin by calculating the system's thermodynamic properties, including entropy, heat capacity, and *Hawking* radiation. For the latter, we use two distinct methods: surface gravity and the topological approach. Additionally, we investigate the emission rate and remnant mass in this context. Notably, the black hole's lifetime, post-evaporation, is analytically expressed up to a *grey-body* factor, with estimations made for specific initial and final mass configurations. We also analyze the tensorial quasinormal modes using the 6th-order WKB method. Lastly, we examine the deflection angle, or gravitational lensing, in both the weak and strong deflection limits.

The structure of this work is as follows: In Sec. II, we introduce the general framework of the non-commutative theory under consideration, including the mass distribution, black hole solution, and horizons. In Sec. III A, we discuss the thermodynamics, evaporation, and emission rate. Sec. III A also covers the calculation of the *quasinormal* modes using tensorial perturbations. In Sec. V, we present gravitational lensing calculations in the weak deflection angle limit via the Gauss-Bonnet theorem. In Sec. VI, we revisit gravitational lensing using the strong deflection limit technique. Finally, in Sec. VII, we offer our concluding remarks.

II. THE GENERAL SETUP

Examining the implications of spacetime involves, for instance, taking into account non-commutativity principles with general relativity [111–119]. Various formulations of non-commutative field theory, based on the Moyal product, have been proposed [120]. This section initiates by examining key features of the black hole solution in question, beginning with the provided distribution [15, 119, 121]

$$\rho_{\Theta}(r) = \frac{M\sqrt{\Theta}}{\pi^{3/2}(r^2 + \pi\Theta)^2}, \quad (1)$$

where M is the total mass and Θ is the non-commutative parameter with dimension of $[L^2]$, which is defined as

$$[x^{\mu}, x^{\nu}] = i\Theta^{\mu\nu}. \quad (2)$$

In Fig. 1, we represent the distribution $\rho_{\Theta}(r)$, considering different values of the non-commutative parameter Θ . Here, we can also define \mathcal{M}_{Θ} as

$$\mathcal{M}_{\Theta} = \int_0^r 4\pi r^2 \rho_{\Theta}(r) dr = M - \frac{4M\sqrt{\Theta}}{\sqrt{\pi}r}. \quad (3)$$

In possession of it, in the non-commutative scenario, the Schwarzschild-like black hole is

$$ds^2 = -f_{\Theta}(r)dt^2 + f_{\Theta}(r)dr^2 + r^2 d\theta^2 + r^2 \sin^2 \theta d\varphi^2, \quad (4)$$

in which

$$f_{\Theta}(r) = 1 - \frac{2M}{r} + \frac{8M\sqrt{\Theta}}{\sqrt{\pi}r^2}. \quad (5)$$

Such a metric gives rise to two physical solutions

$$r_{\pm} = M \pm \frac{\sqrt{\pi M^2 - 8\sqrt{\pi}\sqrt{\Theta}M}}{\sqrt{\pi}}, \quad (6)$$

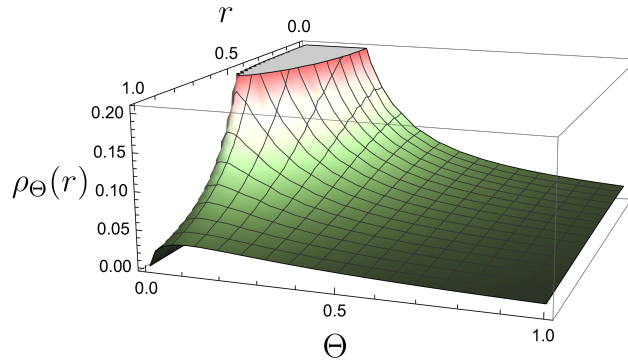


Figure 1: The representation of the distribution $\rho_{\Theta}(r)$.

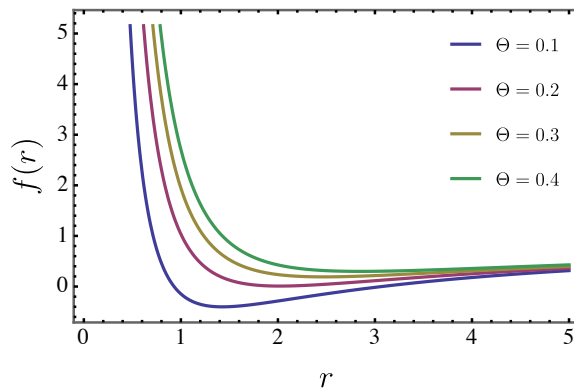


Figure 2: The representation of $f(r)$ for different values of Θ .

and

$$r_- = M - \frac{\sqrt{\pi M^2 - 8\sqrt{\pi}\sqrt{\Theta}M}}{\sqrt{\pi}}, \quad (7)$$

where r_+ and r_- are the event the Cauchy horizon respectively. To enhance reader comprehension, we present plots and tables illustrating both quantities. Fig. 2 depicts r_+ and r_- as functions of M for various values of Θ . Furthermore, Tab. I reveals that as M increases, so does r_+ , while an increase in Θ corresponds to a decrease in the radius of the event horizon. Conversely, Tab. II demonstrates that as mass increases, r_- decreases; additionally, an increase in the non-commutative parameter results in a growth of the radius of the Cauchy horizon.

Table I: The event horizon, r_+ , is shown for a range of values of mass M , and parameter Θ .

M	Θ	r_+	M	Θ	r_+
0.00	0.01	0.00000	2.00	0.00	4.00000
1.00	0.01	1.74071	2.00	0.01	3.75991
2.00	0.01	3.75991	2.00	0.02	3.65027
3.00	0.01	5.76513	2.00	0.03	3.56092
4.00	0.01	7.76757	2.00	0.04	3.48142
5.00	0.01	9.76899	2.00	0.05	3.40766
6.00	0.01	11.7699	2.00	0.06	3.33747
7.00	0.01	13.7706	2.00	0.07	3.26952
8.00	0.01	15.7710	2.00	0.08	3.20282
9.00	0.01	17.7714	2.00	0.09	3.13661
10.0	0.01	19.7717	2.00	0.10	3.07023

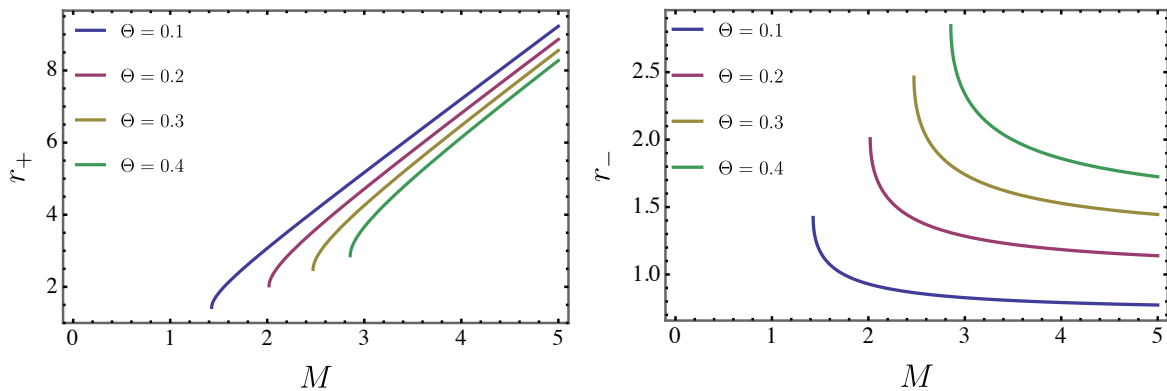


Figure 3: The event (on the left panel) and the Cauchy (on the right panel) are shown for different values of Θ .

Table II: The Cauchy horizon, r_- , is shown for a range of values of mass M , and parameter Θ .

M	Θ	r_-	M	Θ	r_-
0.00	0.01	0.000000	2.00	0.00	0.000000
1.00	0.01	0.259292	2.00	0.01	0.240086
2.00	0.01	0.240086	2.00	0.02	0.349732
3.00	0.01	0.234870	2.00	0.03	0.439080
4.00	0.01	0.232429	2.00	0.04	0.518584
5.00	0.01	0.231013	2.00	0.05	0.592345
6.00	0.01	0.230088	2.00	0.06	0.662526
7.00	0.01	0.229436	2.00	0.07	0.730484
8.00	0.01	0.228952	2.00	0.08	0.797183
9.00	0.01	0.228579	2.00	0.09	0.863387
10.0	0.01	0.228281	2.00	0.10	0.929766

III. THERMODYNAMICS, EVAPORATION AND EMISSION RATE

In this section, we shall analyze the thermodynamic behavior of the system and the respective evaporation process; also, we shall estimate the lifetime of the black hole under consideration.

A. Hawking temperature via topological method

Using the topological technique, one can determine the Hawking temperature without sacrificing the knowledge about the higher-dimensional space by using the Euclidean geometry of the 2-dimensional spacetime. The thermodynamic property of Hawking temperature for a two-dimensional black hole can be established using the topological method [122–124]

$$T_H = \frac{\hbar c}{4\pi\chi k_B} \sum_{j \leq \chi} \int_{r_{h_j}} \sqrt{|g|} \mathcal{R} dr. \quad (8)$$

In this context, the symbols \hbar , c , and k_B represent the Planck constant, speed of light, and Boltzmann's constant, respectively. Additionally, g corresponds to the metric determinant, and r_{h_j} signifies the j -th Killing horizon. For this study, we adopt the values $\hbar = 1$, $c = 1$, and $k_B = 1$ for these parameters. The function \mathcal{R} denotes the Ricci scalar in the two-dimensional spacetime. The variable χ represents the Euler characteristic of the Euclidean geometry and is linked to the count of Killing horizons. The symbol $\sum_{j \leq \chi}$ signifies the summation across the Killing horizons.

The Euler characteristic in a two-dimensional spacetime is expressed as follows:

$$\chi = \int \sqrt{|g|} d^2x \frac{\mathcal{R}}{4\pi}. \quad (9)$$

Upon employing the Wick rotation $t = i\tau$ and defining the new compact time as the inverse temperature β , the Euler characteristic χ takes the form [122, 123].

$$\chi = \int_0^\beta d\tau \int_{r_H} \sqrt{|g|} dr \frac{\mathcal{R}}{4\pi}. \quad (10)$$

Subsequently, the connection between the Hawking temperature T_H and the Euler characteristic χ is established through the relation:

$$\frac{1}{4\pi T_H} \int_{r_H} \sqrt{|g|} \mathcal{R} dr = \chi, \quad (11)$$

this relationship serves as the basis for Eq. (8).

By considering a specific hypersurface, the black hole can be transformed into a two-dimensional configuration with a reduced metric [125] through the Wick rotation ($\tau = it$):

$$ds^2 = f_\Theta(r) d\tau^2 + \frac{dr^2}{f_\Theta(r)}. \quad (12)$$

The Ricci scalar corresponding to the reduced metric (12) is given by:

$$\mathcal{R} = \frac{4M}{r^3} - \frac{48\sqrt{\Theta}M}{\sqrt{\pi}r^4}. \quad (13)$$

Hence, the temperature of the black hole is determined by employing the formula:

$$T_\Theta = \frac{1}{4\pi\chi} \int_{r_+} \sqrt{|g|} \mathcal{R} dr = \frac{M}{2\pi r_+^2} - \frac{4\sqrt{\Theta}M}{\pi^{3/2} r_+^3}, \quad (14)$$

which leads to the same result by using the surface gravity formula

$$T_\Theta = \frac{1}{4\pi\sqrt{g_{00}g_{11}}} \left. \frac{dg_{00}}{dr} \right|_{r=r_+} = \frac{M}{2\pi r_+^2} - \frac{4\sqrt{\Theta}M}{\pi^{3/2} r_+^3}, \quad (15)$$

where M is obtained if we consider $f(r_+) = 0$, which reads

$$M = \frac{r_+^2}{2\left(r_+ - \frac{4\sqrt{\Theta}}{\sqrt{\pi}}\right)}. \quad (16)$$

Explicitly, in terms of the horizon, such a thermal quantity is given by

$$T_\Theta = \frac{1}{2\pi r_+ \left(\frac{r_+}{r_+ - \frac{4\sqrt{\Theta}}{\sqrt{\pi}}} + 1 \right)}. \quad (17)$$

To visualize better the *Hawking* temperature, we present Fig. 4, regarding different ranges of the event horizon and the non-commutative parameter. Notably, note that, for small values of r_+ , such a thermodynamic function indicates a phase transition, as displayed in the left panel. In general lines, Θ decreases as the magnitude of T_Θ grows, as seen in the right panel. Moreover, we compare our results with the Schwarzschild case and another one, which was recently obtained within the context of non-commutative gauge theory [9].

B. Entropy

Another thermodynamic quantity worthy to be investigated is indeed the entropy. Therefore, the area of the event horizon can be cast as:

$$A_\Theta = \int \int \sqrt{g_{22}g_{33}} d\theta d\varphi = 4\pi r_+^2. \quad (18)$$

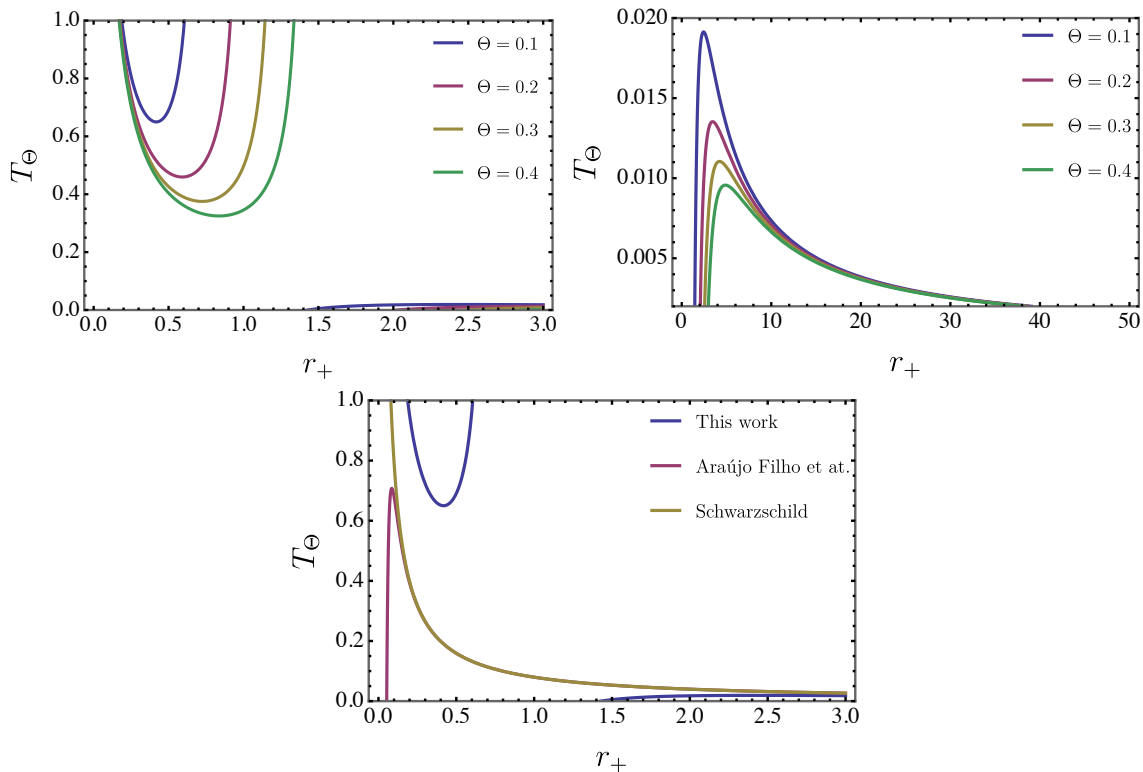


Figure 4: The *Hawking* temperature are shown for different ranges of r_+ and Θ .

From this result, we can properly compute the entropy, as shown below

$$S_{\Theta} = \frac{A_{\Theta}}{4} = \pi \left(\frac{\sqrt{M(\sqrt{\pi}M - 8\sqrt{\Theta})}}{\sqrt[4]{\pi}} + M \right)^2. \quad (19)$$

In Fig. 5, we show the entropy behavior, considering distinct values of the mass and parameter Θ . As we can see, the second law of thermodynamics is also verified for our black hole solution. Furthermore, we compare our outcomes with the Schwarzschild case and Ref. [9].

C. Heat capacity

Finally, let us address the heat capacity

$$C_{\Theta V} = T_{\Theta} \frac{\partial S_{\Theta}}{\partial T_{\Theta}} = T_{\Theta} \frac{\partial S_{\Theta}/\partial M}{\partial T_{\Theta}/\partial M} = 2\pi r_+^2 \left(\frac{1}{4 - \frac{32\Theta + \pi r_+^2}{4\sqrt{\pi}\sqrt{\Theta}r_+}} - 1 \right). \quad (20)$$

In Fig. 6, the behavior of the heat capacity analogously to what we have accomplished up to now is exhibited. Notice that several phase transitions are also highlighted in such a plot. Also, we provide a comparative analysis of our findings regarding both the Schwarzschild case and recent literature [9]. Finally, to display a general panorama of all thermodynamic functions, we present Tab. III. Here, we compare all thermal quantities developed in this work with Schwarzschild and the results shown in Ref. [9].

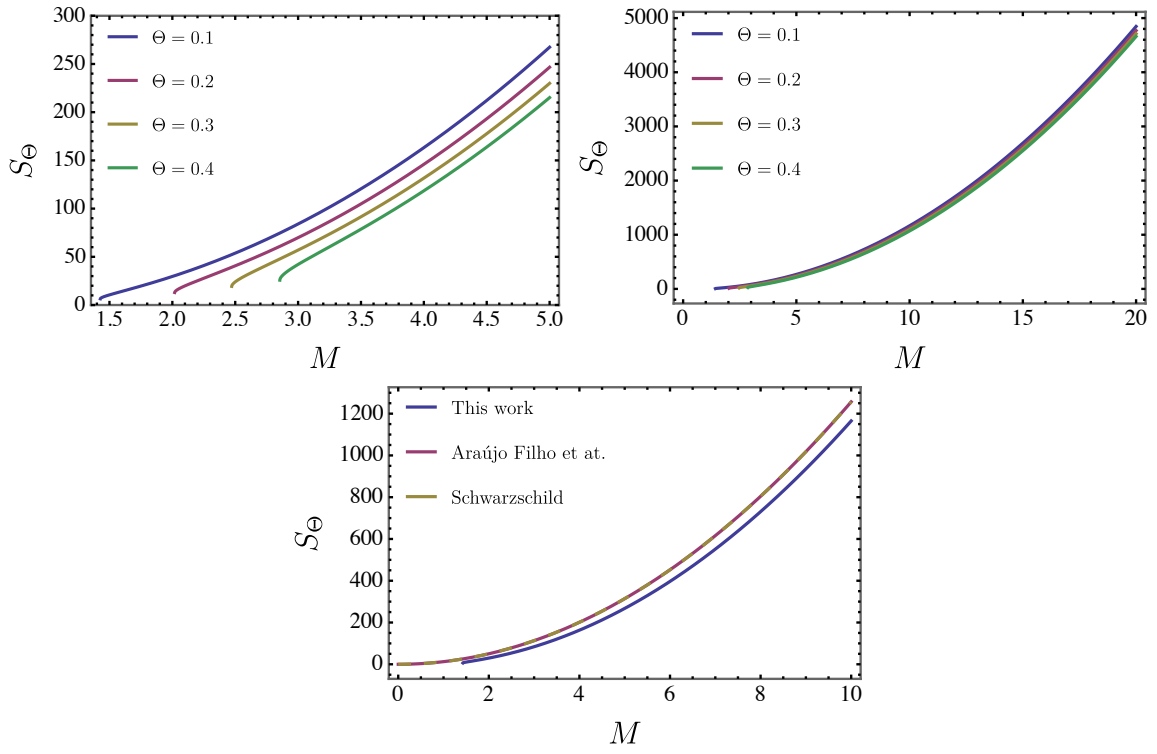


Figure 5: The entropy is exhibited for different ranges of M and Θ .

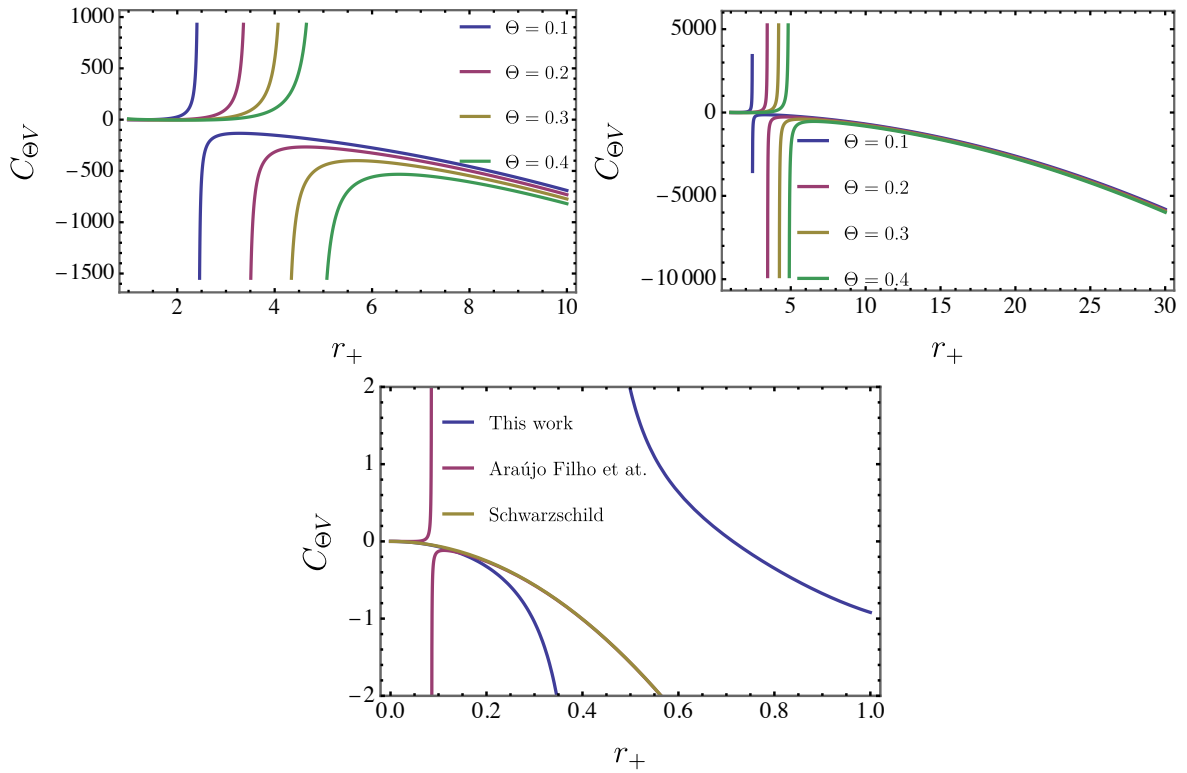


Figure 6: The heat capacity is displayed for different ranges of M and Θ .

Table III: Comparison of the thermodynamic properties between a NC Schwarzschild BH obtained by the present study (via deformed mass) and the previous results (from deformed metric). Here,

$$\Gamma = 32\pi r_+^2 \left(\Theta^2 - 2r_+^2 + \sqrt{\Theta^4 + 4r_+^4 + 7\Theta^2 r_+^2} \right)^2, \text{ and } r_s \text{ is the Schwarzschild radius.}$$

	This work	Araújo Filho et al. [9]	Schwarzschild
T_Θ	$\frac{1}{2\pi r_+ \left(\frac{r_+}{r_+ - \frac{2\sqrt{\Theta}}{\pi}} + 1 \right)}$	$\frac{11\Theta^2 \left(256r_+^2 \left(\Theta^2 - 2r_+^2 + \sqrt{\Theta^4 + 4r_+^4 + 7\Theta^2 r_+^2} \right)^2 - 363\Theta^6 \right)}{4096\pi r_+^3 \left(\Theta^2 - 2r_+^2 + \sqrt{\Theta^4 + 4r_+^4 + 7\Theta^2 r_+^2} \right)^3}$	$\frac{1}{4\pi r_s}$
A_Θ	$4\pi r_+^2$	$4\pi r_s^2 + \frac{5\pi}{16}\Theta^2$	$4\pi r_s^2$
S_Θ	πr_+^2	$\pi r_s^2 + \frac{5\pi}{64}\Theta^2$	πr_s^2
$C_{V\Theta}$	$2\pi r_+^2 \left(\frac{1}{4 - \frac{32\Theta + \pi r_+^2}{4\sqrt{\pi}\sqrt{\Theta}r_+}} - 1 \right)$	$\Gamma \left(\frac{256r_+^2 \left(\Theta^2 - 2r_+^2 + \sqrt{\Theta^4 + 4r_+^4 + 7\Theta^2 r_+^2} \right)^2}{121\Theta^4} - 3\Theta^2 \right)$ $- \frac{121\Theta^4 \left(\frac{256r_+^2 \left(\Theta^2 - 2r_+^2 + \sqrt{\Theta^4 + 4r_+^4 + 7\Theta^2 r_+^2} \right)^2}{121\Theta^4} - 9\Theta^2 \right)}{121\Theta^4}$	$-2\pi r_s^2$

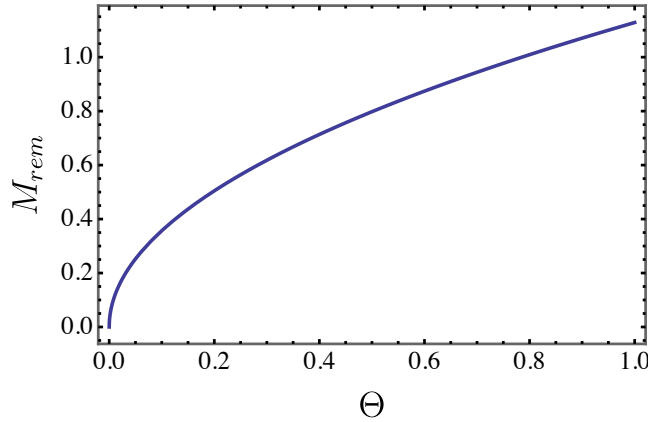


Figure 7: M_{rem} as a function of the non-commutative parameter Θ .

D. Evaporation process

Now, let us examine the evaporation process of our non-commutative black hole. To do so, it is reasonable to calculate the remnant mass, M_{rem} . Note that, in our scenario, as the black hole approaches its final stage of evaporation ($T_\Theta \rightarrow 0$), this culminates in the following expression to the mass

$$M_{rem} = \frac{2\sqrt{\Theta}}{\sqrt{\pi}}. \quad (21)$$

From the aforementioned equation, it is clear that only one parameter, namely Θ , exerts influence on the modification of M_{rem} . To facilitate a comprehensive understanding of the behavior of this mass, we present Fig. 7. Another important aspect worth exploring in this context is essentially the black hole lifetime. Thereby, we have

$$\frac{dM}{d\tau} = -\alpha\sigma a T_\Theta^4. \quad (22)$$

Here, a represents the radiation constant, σ denotes the cross-sectional area, and α is for the greybody factor. Taking into consideration the geometric optics approximation, σ is thereby understood as the cross section for photon capture:

$$\sigma = \pi \left(\frac{g_{\varphi\varphi}}{g_{tt}} \right) \Big|_{r=r_{ph}} = \frac{\left(\sqrt{M \left(9\sqrt{\pi}M - 64\sqrt{\Theta} \right)} + 3\sqrt[4]{\pi}M \right)^4}{8 \left(3\pi M^2 - 16\sqrt{\pi}\sqrt{\Theta}M + \pi^{3/4}M \sqrt{M \left(9\sqrt{\pi}M - 64\sqrt{\Theta} \right)} \right)}, \quad (23)$$

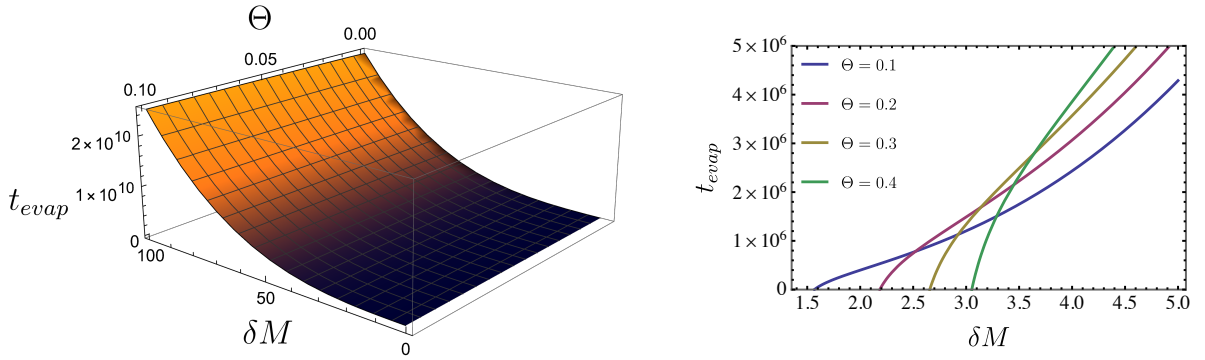


Figure 8: The evaporation time, denoted as t_{evap} , as a function of M and Θ on the left hand; also, it is also displayed t_{evap} , regarding some fixed values of Θ as a function of M .

where r_{ph} is the photon sphere radius given by

$$r_{ph} = \frac{\left(\sqrt{M \left(9\sqrt{\pi}M - 64\sqrt{\Theta} \right)} + 3\sqrt[4]{\pi}M \right)^4}{8 \left(3\pi M^2 - 16\sqrt{\pi}\sqrt{\Theta}M + \pi^{3/4}M\sqrt{M \left(9\sqrt{\pi}M - 64\sqrt{\Theta} \right)} \right)}. \quad (24)$$

With this, we can substitute these previous expressions in Eq. (22), so that

$$\frac{dM}{d\tau} = \frac{-\xi M \left(\sqrt{\pi}M - 8\sqrt{\Theta} \right)^2}{8\pi^{7/2} \left(\sqrt{M \left(\sqrt{\pi}M - 8\sqrt{\Theta} \right)} + \sqrt[4]{\pi}M \right)^4 \left(-16\sqrt{\Theta} + \sqrt[4]{\pi}\sqrt{M \left(9\sqrt{\pi}M - 64\sqrt{\Theta} \right)} + 3\sqrt{\pi}M \right)}, \quad (25)$$

where $\xi = a\alpha$. Therefore, we have to solve

$$\int_0^{t_{evap}} \xi d\tau = \int_{M_i}^{M_{rem}} dM \left[\frac{-\xi M \left(\sqrt{\pi}M - 8\sqrt{\Theta} \right)^2}{8\pi^{7/2} \left(\sqrt{M \left(\sqrt{\pi}M - 8\sqrt{\Theta} \right)} + \sqrt[4]{\pi}M \right)^4 \kappa} \right]^{-1}, \quad (26)$$

where M_i is the initial mass configuration, t_{evap} being the time for reaching the final stage of the respective its evaporation, and $\kappa = \left(-16\sqrt{\Theta} + \sqrt[4]{\pi}\sqrt{M \left(9\sqrt{\pi}M - 64\sqrt{\Theta} \right)} + 3\sqrt{\pi}M \right)$. Therefore, we obtain the general expression for t_{evap} , as shown in the Appendix. Now, let us estimate the lifetime of the black hole under consideration for a particular configuration of M_i (initial mass) and M_f (final mass). For instance, if $M_i = 10$ and $M_f = M_{rem} = 0.356825$ (for $\Theta = 0.001$), we get

$$t_{evap} = \frac{1}{\xi} (2.51807 \times 10^7). \quad (27)$$

In Fig. 9, we show the reduction of mass M until reaching the final state of the black hole evaporation, i.e., when it reaches its remnant mass M_{rem} .

E. Emission rate

Subsequently, our focus shifts to determining the rate of energy emission by black holes, commonly referred to as *Hawking* radiation. It is established that the black hole shadow corresponds to its high energy absorption cross-section

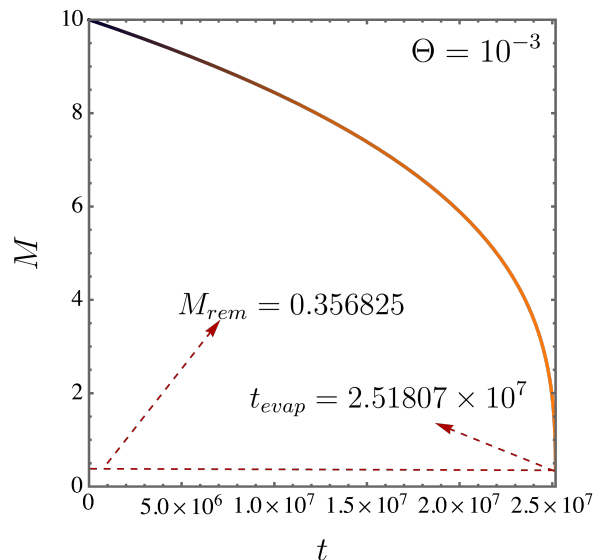


Figure 9: The reduction of mass as a function of time.

for observers at infinity. Conversely, at higher energies, it converges to a constant value known as σ_{lim} , which, for a spherically symmetric black hole, is described in [126].

$$\sigma_{lim} \approx R_{sh}^2. \quad (28)$$

Applying such a limit, the computation of the rate of energy emission of a black hole is then performed[126–129]

$$\frac{d^2 E}{d\omega dt} = \frac{2\pi^2 \sigma_{lim}}{e^{\omega/T_\Theta} - 1} \omega^3, \quad (29)$$

with ω represents the photon frequency.

Figure 10 illustrates the emission rate plotted against the frequency ω for different values of Θ . It is evident that as frequencies tend towards both zero and infinity, the emission rate diminishes. Additionally, it is noteworthy that Θ contributes to diminishing the magnitude of the emission rate.

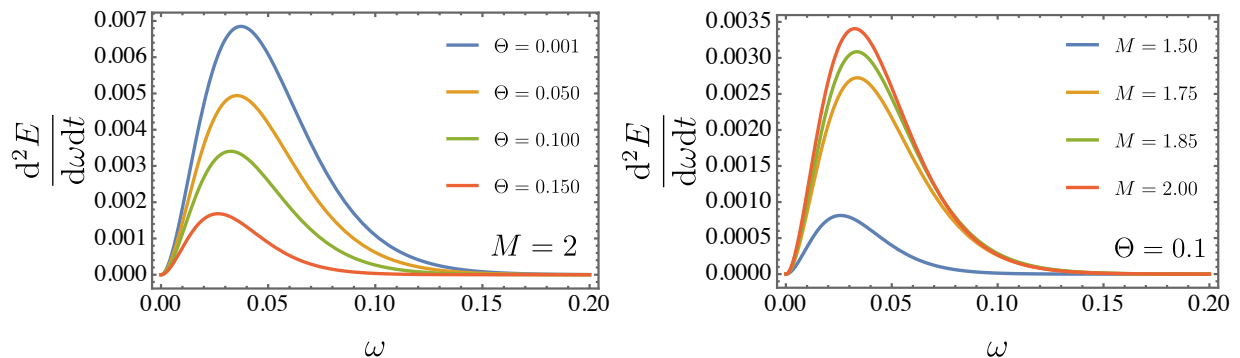


Figure 10: The emission rate for distinct patterns of Θ and M .

IV. QUASINORMAL MODES

A noteworthy phenomenon termed *quasinormal* modes emerges, revealing distinct oscillation patterns that remain largely unaltered by initial perturbations. These modes exemplify the inherent characteristics of the system, deriving

from the natural oscillations of spacetime, irrespective of specific initial conditions. Unlike *normal* modes associated with closed systems, *quasinormal* modes correspond to open systems, gradually dissipating energy through the emission of gravitational waves. Mathematically, they are characterized as poles of the complex Green function.

To ascertain their frequencies, researchers derive solutions to the wave equation within a system governed by the background metric $g_{\mu\nu}$. However, obtaining analytical solutions for these modes frequently poses significant challenges. Various methodologies have been explored in scientific literature to address this issue. Among these, the WKB (Wentzel-Kramers-Brillouin) method stands out as particularly prevalent. Its origins can be traced back to the seminal contributions of Will and Iyer [130, 131]. Subsequent advancements, including extensions up to the sixth order by Konoplya [132] and up to the thirteenth order by Matyjasek and Opala [133], have further refined this approach.

In particular, this section is dedicated to exploring the *quasinormal* modes specifically in the context of tensorial (gravitational) perturbations. Our focus will align closely with the findings of Ref. [35, 134]. In general lines, the axially symmetric spacetime can be expressed as:

$$ds^2 - e^{2\nu} dt^2 + e^{2\psi} (d\phi - q_1 dt - q_2 dr - q_3 d\theta)^2 e^{2\mu_2} dr^2 + e^{2\mu_3} d\theta^2. \quad (30)$$

Taking into account the non-perturbed black hole, we obtain

$$e^{2\nu} = f(r), \quad e^{-2\mu_2} = \left(1 - \frac{2m(r)}{r}\right) = \frac{\Delta}{r^2}, \quad (31)$$

in which

$$\Delta = r^2 - 2m(r)r, \quad e^{\mu_3} = r, \quad e^\psi = r \sin \theta, \quad (32)$$

and

$$q_1 = q_2 = q_3 = 0, \quad (33)$$

where the metric presented in (4) can properly be written as follows

$$f_\Theta(r) = 1 - \frac{2\mathcal{M}_\Theta(r)}{r}, \quad (34)$$

so that

$$\mathcal{M}_\Theta(r) = M - \frac{4M\sqrt{\Theta}}{\sqrt{\pi}r}.$$

Axial perturbations are commonly characterized by q_1 , q_2 , and q_3 . It is worth noting that for the linear perturbations $\delta\nu$, $\delta\psi$, $\delta\mu_2$, $\delta\mu_3$, polar ones with even parity emerge. However, such perturbations fall outside the scope of this paper. Now, turning our attention to Einstein's equations, we find

$$(e^{3\psi+\nu-\mu_2-\mu_3} Q_{23})_{,3} = -e^{3\psi-\nu-\mu_2+\mu_3} Q_{02,0}, \quad (35)$$

where $x^2 = r$, $x^3 = \theta$ and $Q_{AB} = q_{A,B} - q_{B,A}$, $Q_{A0} = q_{A,0} - q_{1,A}$ [35, 134]. In addition, we can also rewrite the above expression as

$$\frac{\sqrt{f(r)}}{\sqrt{\Delta}} \frac{1}{r^3 \sin^3 \theta} \frac{\partial Q}{\partial \theta} = -(q_{1,2} - q_{2,0})_{,0}, \quad (36)$$

in which Q is given as

$$Q(t, r, \theta) = \Delta Q_{23} \sin^3 \theta = \Delta (q_{2,3} - q_{3,2}) \sin^3 \theta. \quad (37)$$

Considering another significant equation, namely,

$$(e^{3\psi+\nu-\mu_2-\mu_3} Q_{23})_{,2} = e^{3\psi-\nu+\mu_2-\mu_3} Q_{03,0}, \quad (38)$$

it can be shown that

$$\frac{\sqrt{f(r)}\sqrt{\Delta}}{r^3 \sin^3 \theta} \frac{\partial Q}{\partial \theta} = (q_{1,3} - q_{3,0})_{,0}. \quad (39)$$

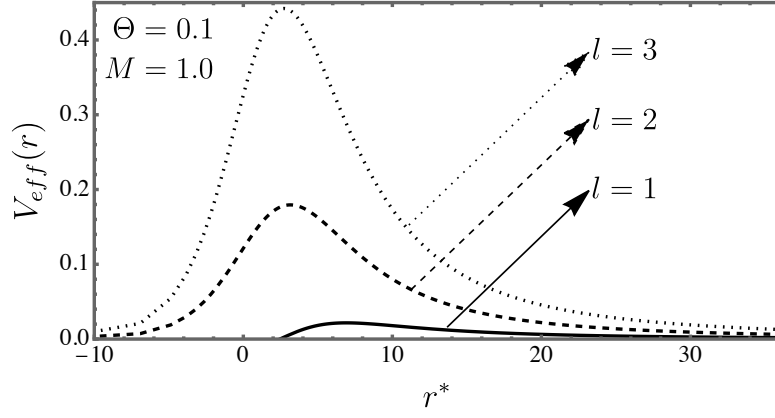


Figure 11: The effective potential $V_{eff}(r)$ is shown as a function of the tortoise coordinate r^* for tensorial perturbations.

We can demonstrate this further by employing the expression $Q(r, \theta) = Q(r)C_{l+2}^{-3/2}(\theta)$, where $C_n^\nu(\theta)$ denotes the Gegenbauer function that obeys [35, 134],

$$\left[\frac{d}{d\theta} \sin^{2\nu} \theta \frac{d}{d\theta} + n(n+2\nu) \sin^{2\nu} \theta \right] C_n^\nu(\theta) = 0, \quad (40)$$

therefore

$$r\sqrt{f(r)\Delta} \frac{d}{dr} \left(\frac{\sqrt{f(r)\Delta}}{r^3} \frac{dQ}{dr} \right) - \mu^2 \frac{f(r)}{r^2} Q + \omega^2 Q = 0, \quad (41)$$

where $\mu^2 = (l-1)(l+2)$. Here, we regard $Q = rZ$ so that $\frac{d}{dr^*} = \sqrt{f(r)\Delta} \frac{1}{r} \frac{d}{dr}$, and

$$\left(\frac{d^2}{dr^{*2}} + \omega^2 - V_{eff}(r) \right) Z = 0, \quad (42)$$

with r^* being the tortoise coordinate. Explicitly, it reads

$$r^* = r + M \ln \left(8\sqrt{\Theta}M + \sqrt{\pi}r(r-2M) \right) + \frac{2\sqrt{M} \left(\sqrt{\pi}M - 4\sqrt{\Theta} \right) \tanh^{-1} \left(\frac{\sqrt[4]{\pi}(M-r)}{\sqrt{M}\sqrt{\sqrt{\pi}M-8\sqrt{\Theta}}} \right)}{\sqrt[4]{\pi}\sqrt{\sqrt{\pi}M-8\sqrt{\Theta}}}. \quad (43)$$

Furthermore, the effective potential can properly be obtained

$$V_{eff}(r) = f_\Theta(r) \left(\frac{l(l+1)}{r^2} - \frac{6\mathcal{M}_\Theta(r)}{r^3} + \frac{2\mathcal{M}'_\Theta(r)}{r^2} \right), \quad (44)$$

in such a way that

$$V_{eff}(r) = f_\Theta(r) \left(\frac{l(l+1)}{r^2} + \frac{2M \left(\frac{16\sqrt{\Theta}}{\sqrt{\pi}} - 3r \right)}{r^4} \right). \quad (45)$$

As it is usually inferred in the studies of *quasinormal* modes, we provide the plots of the effective potential $V_{eff}(r)$ against the tortoise coordinate r^* in Fig. 11. Here, the graphic is performed by considering particular values of $\Theta = 0.1$ and $M = 1.0$ for different values of l .

Effectively solving Eq. (42) requires carefully considering the relevant boundary conditions. In our particular scenario, solutions stand out by demonstrating purely ongoing behavior near the horizon

$$Z^{\text{in}}(r^*) \sim \begin{cases} C_l(\omega)e^{-i\omega r^*} & (r^* \rightarrow -\infty) \\ A_l^{(-)}(\omega)e^{-i\omega r^*} + A_l^{(+)}(\omega)e^{+i\omega r^*} & (r^* \rightarrow +\infty). \end{cases}$$

Spin 2	$l = 0$	$l = 1$	$l = 2$
Θ	ω_0	ω_0	ω_0
0.10	4.84572 - 5.88427i	4.18317 - 5.95134i	2.89163 - 6.04328i
0.12	4.02939 - 4.82192i	3.42490 - 4.88470i	2.24718 - 4.97041i
0.14	3.44481 - 4.07124i	2.88527 - 4.13141i	1.79907 - 4.20667i
0.16	3.00574 - 3.51331i	2.48475 - 3.56838i	1.47109 - 3.63607i
0.18	2.66628 - 3.08019i	2.17584 - 3.13252i	1.22090 - 3.19606i
0.20	2.39581 - 2.73483i	1.93000 - 2.78633i	1.02532 - 2.84456i

Table IV: The *quasinormal* modes are shown by using sixth-order WKB approximation, considering different values of Θ . Here, the multipole numbers are regarded $l = 0$, $l = 1$, and $l = 2$.

The integral complex coefficients $A_l^{(+)}(\omega)$, $C_l(\omega)$, and $A_l^{(-)}(\omega)$ are considered crucial for our subsequent analytical investigation. They are utilized as fundamental elements in the examination of the *quasinormal* modes associated with a black hole, distinguished by frequencies ω_{nl} , satisfying the condition $A_l^{(-)}(\omega_{nl}) = 0$. These modes are characterized by a distinctive behavior, with purely outgoing waves observed at spatial infinity and exclusively ongoing waves near the event horizon. The integers n and l are denoted as the overtone and multipole numbers, respectively. Furthermore, it is noteworthy that the spectrum of *quasinormal* modes represents the eigenvalues derived from Eq. (42). In order to provide the calculation of these frequencies, the WKB method, a semi-analytical technique reminiscent of quantum mechanics, is invoked.

Moreover, the WKB approximation, which Schutz and Will introduced [135], has become a remarkable method to address the *quasinormal* modes, particularly in analyzing particle scattering around black holes. This technique has undergone refinement over the years, with significant contributions from Konoplya [132, 136]. However, it is crucial to recognize that the method's applicability relies on the potential exhibiting a barrier-like structure (as shown in Fig. 11) and leveling off to constant values as $r^* \rightarrow \pm\infty$. By aligning the solution power series with the peak potential turning points, researchers can accurately derive the *quasinormal* modes [137]. Given these premises, the expression for the sixth-order WKB formula is as follows:

$$\frac{i(\omega_n^2 - V_0)}{\sqrt{-2V_0''}} - \sum_{j=2}^6 \Lambda_j = n + \frac{1}{2}. \quad (46)$$

In essence, Konoplya's formulation for the *quasinormal* modes comprises several key components. In particular, the term V_0'' represents the second derivative of the potential, evaluated at its maximum r_0 . Furthermore, the constants Λ_j are influenced by the effective potential and its derivatives at this peak. Notably, recent progress in this field has revealed a 13th-order WKB approximation developed by Matyjasek and Opala [133].

It is to be noted that the *quasinormal* frequencies are characterized by a negative imaginary component. This feature implies that these modes are subject to exponential decay over time, indicating energy dissipation through gravitational waves. This observation is in line with previous studies examining scalar, electromagnetic, and gravitational perturbations within spherically symmetric contexts [35, 55, 138–140].

In Tab. IV, we present the *quasinormal* modes for a variety of values of Θ ; also, we have considered $l = 0$, $l = 1$, and $l = 2$. In general lines, the non-commutative parameter is responsible for attenuating the dumped frequencies. Similar conclusions were addressed recently in the literature, concerning distinct methods to introduce the non-commutativity in gravity [141, 142].

V. WEAK DEFLECTION ANGLE USING GAUSS-BONNET THEOREM

In this section, we review the Gauss-Bonnet theorem and compute the weak deflection angle of the black hole. Initially, we express the null geodesics satisfying $ds^2 = 0$, a rearrangement of which yields:

$$dt^2 = \gamma_{ij} dx^i dx^j = \frac{1}{f_{\Theta}(r)^2} dr^2 + \frac{r^2}{f_{\Theta}(r)} d\Omega^2, \quad (47)$$

Here, i and j range from 1 to 3, and γ_{ij} represents the optical metric.

To employ the Gauss-Bonnet theorem, it is imperative to compute the Gaussian curvature, and this calculation is performed here:

$$\mathcal{K} = \frac{R}{2} = \frac{f_{\Theta}(r)}{2} \frac{d^2}{dr^2} f_{\Theta}(r) - \frac{\left(\frac{d}{dr} f_{\Theta}(r)\right)^2}{4} = \frac{128\Theta M^2}{\pi r^6} - \frac{48\sqrt{\Theta} M^2}{\sqrt{\pi} r^5} + \frac{3M^2}{r^4} + \frac{24\sqrt{\Theta} M}{\sqrt{\pi} r^4} - \frac{2M}{r^3}. \quad (48)$$

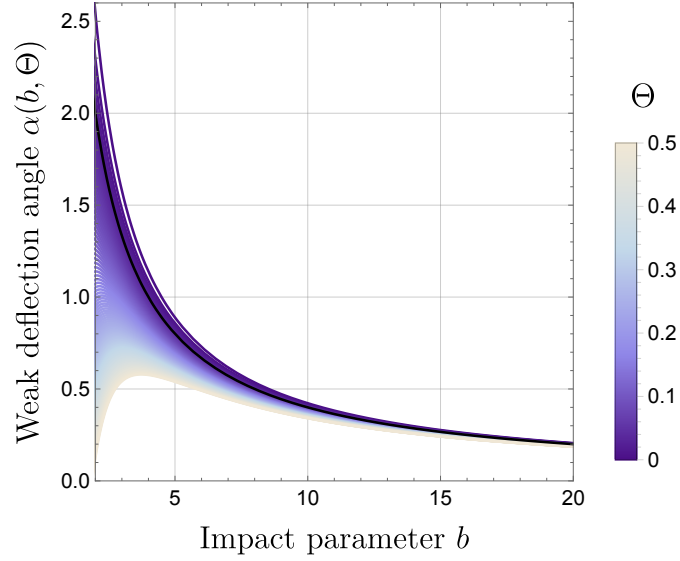


Figure 12: Weak deflection angle α versus impact parameter b for $M = 1$ and variable Θ . The black solid line is for the Schwarzschild case.

Here, $\gamma \equiv \det(\gamma_{ij})$, and R represents the Ricci scalar. The surface area on the equatorial plane is expressed as [143]:

$$dS = \sqrt{\gamma} dr d\phi = \frac{r}{f_{\Theta}(r)^{3/2}} dr d\phi \approx \left(r + \frac{3M(\sqrt{\pi}r - 4\sqrt{\Theta})}{\sqrt{\pi}r} \right) dr d\phi. \quad (49)$$

Subsequently, the deflection angle of light can be computed as:

$$\begin{aligned} \alpha &= - \int \int_{\bar{D}} \mathcal{K} dS = - \int_0^{\pi} \int_{\frac{b}{\sin \phi}}^{\infty} \mathcal{K} dS \\ &\simeq \frac{4M}{b} + \frac{15\Theta M^2}{b^4} - \frac{64\sqrt{\Theta} M^2}{3\sqrt{\pi} b^3} + \frac{3\pi M^2}{4b^2} - \frac{6\sqrt{\pi}\sqrt{\Theta} M}{b^2}. \end{aligned} \quad (50)$$

In this calculation, the zero-order particle trajectory $r = b/\sin \phi$, where $0 \leq \phi \leq \pi$ in the weak deflection limit, has been employed which is shown in Fig. 12. As Θ increases from 0 to 0.5, the deflection angle α decreases. This suggests that higher values of Θ reduce the deflection angle, indicating a weaker gravitational lensing effect. For larger b values, the deflection angle is predominantly influenced by the leading term $\frac{4M}{b}$. The differences due to varying Θ become less pronounced in this range. At smaller b values, the higher-order terms involving Θ and M^2 become more significant, resulting in noticeable differences in the deflection angle for different Θ values. The plot effectively illustrates the impact of Θ on the deflection angle, showing that higher Θ values lead to a smaller deflection angle for light passing near the black hole.

VI. GRAVITATIONAL LENSING IN THE STRONG DEFLECTION LIMIT

In this section, we describe the general methodology used to obtain the deflection angle of a light ray within the strong deflection limit [144]. Like many previous works (e.g., [145, 146]), we focus on asymptotically flat, static, and spherically symmetric spacetimes characterized by the line element:

$$ds^2 = -A(r)dt^2 + B(r)dr^2 + C(r)(d\theta^2 + \sin^2 \theta d\phi^2). \quad (51)$$

To apply the method proposed by Tsukamoto [144], the metric must satisfy the asymptotic flatness condition. Specifically, the coefficients $A(r)$, $B(r)$, and $C(r)$ should behave as follows: $\lim_{r \rightarrow \infty} A(r) = 1$, $\lim_{r \rightarrow \infty} B(r) = 1$, and $\lim_{r \rightarrow \infty} C(r) = r^2$. Due to the spacetime symmetries, there are two Killing vectors: ∂_t and ∂_{ϕ} .

We shall now briefly describe the procedure for calculating the deflection angle in the strong field regime, starting by defining a new variable, $D(r)$:

$$D(r) \equiv \frac{C'(r)}{C(r)} - \frac{A'(r)}{A(r)}, \quad (52)$$

with the prime indices representing the derivative with respect to the radial coordinate. We assume there is at least one positive solution when $D(r) = 0$. The radius of the photon sphere, denoted as r_m , is defined as the largest positive solution of $D(r) = 0$. We assume $A(r)$, $B(r)$, and $C(r)$ are finite and positive for $r \geq r_m$.

Because of the existence of two Killing vectors, there are two conserved quantities: energy $E = A(r)\dot{t}$ and angular momentum $L = C(r)\dot{\phi}$. We assume both E and L are nonzero. With this, we introduce the impact parameter b , defined as:

$$b \equiv \frac{L}{E} = \frac{C(r)\dot{\phi}}{A(r)\dot{t}}. \quad (53)$$

Due to axial symmetry, we can restrict the motion to the equatorial plane ($\theta = \pi/2$), so the radial equation becomes:

$$\dot{r}^2 = V(r), \quad (54)$$

with $V(r) = L^2 R(r)/B(r)C(r)$, and $R(r) \equiv C(r)/A(r)b^2 - 1$. This equation is identical to the motion equation for a unit mass object in a potential $V(r)$. The photon can move where $V(r) \geq 0$. Given the asymptotic flatness conditions, $\lim_{r \rightarrow \infty} V(r) = E^2 > 0$, allowing the photon to exist at infinity ($r \rightarrow \infty$). We assume there is at least one positive solution for $R(r) = 0$.

In this study, we focus on the gravitational lensing scenario where a photon, originating from infinity, approaches a gravitational object, scatters at the closest distance r_0 , and then continues to infinity. For scattering to occur, $r_m < r_0$ must hold, as a photon cannot have a closed orbit in this case. Here, $r = r_0$ is the largest positive solution of $R(r) = 0$, and $B(r)$ and $C(r)$ are finite. Consequently, $V(r)$ vanishes at $r = r_0$. Since r_0 is the point of closest approach where $R(r) = 0$, we deduce:

$$A_0 \dot{t}_0^2 = C_0 \dot{\phi}_0^2. \quad (55)$$

In this manner, and throughout the following discussions, the subscript “0” signifies quantities evaluated at $r = r_0$. For simplicity, we can assume, without loss of generality, that the impact parameter b is positive, especially when dealing with a single light ray. As the impact parameter remains constant along the trajectory, it can be expressed as:

$$b(r_0) = \frac{L}{E} = \frac{C_0 \dot{\phi}_0}{A_0 \dot{t}_0} = \sqrt{\frac{C_0}{A_0}}. \quad (56)$$

Notice that $R(r)$ may also be given by

$$R(r) = \frac{A_0 C}{A C_0} - 1. \quad (57)$$

We outline a condition that is both necessary and sufficient for the existence of a circular light orbit, drawing from the approach as shown in Ref. [147]. Therefore, the trajectory equation reads

$$\frac{BC\dot{r}^2}{E^2} + b^2 = \frac{C}{A}, \quad (58)$$

in such a way that

$$\ddot{r} + \frac{1}{2} \left(\frac{B'}{B} + \frac{C'}{C} \right) \dot{r}^2 = \frac{E^2 D(r)}{AB}. \quad (59)$$

Here, for $r \geq r_m$, $A(r)$, $B(r)$, and $C(r)$ are finite and positive. With E being positive as well, the condition $D(r) = 0$ ensures the consistency of a circular light orbit. It is worth noting that $R'_m = D_m C_m A_m / b^2 = 0$, where the subscript m denotes quantities specifically evaluated at $r = r_m$.

Now, we consider a critical impact parameter, denoted by b_c :

$$b_c(r_m) \equiv \lim_{r_0 \rightarrow r_m} \sqrt{\frac{C_0}{A_0}}. \quad (60)$$

This regard will henceforth be referred to as the strong deflection limit. By taking a derivative of $V(r)$ with respect to r , we have

$$V'(r) = \frac{L^2}{BC} \left[R' + \left(\frac{C'}{C} - \frac{B'}{B} \right) R \right]. \quad (61)$$

This means that as r_0 approaches r_m in the strong deflection limit, both $V(r_0)$ and $V'(r_0)$ tend to zero. Consequently, the trajectory equation adopts the following form:

$$\left(\frac{dr}{d\phi} \right)^2 = \frac{R(r)C(r)}{B(r)}, \quad (62)$$

and the so-called the deflection angle, i.e., $\alpha(r_0)$, can be given by

$$\alpha(r_0) = I(r_0) - \pi, \quad (63)$$

where, in this context, $I(r_0)$ is given by

$$I(r_0) \equiv 2 \int_{r_0}^{\infty} \frac{dr}{\sqrt{\frac{R(r)C(r)}{B(r)}}}. \quad (64)$$

To proceed, our initial task involves taking into account the integration. It is important to mention that such a procedure poses a formidable challenge, as noted in the work by Tsukamoto [144]. In addition, let us define [144]

$$z \equiv 1 - \frac{r_0}{r}, \quad (65)$$

so that the integral is rewritten as

$$I(r_0) = \int_0^1 f(z, r_0) dz, \quad (66)$$

with

$$f(z, z_0) \equiv \frac{2r_0}{\sqrt{G(z, r_0)}}, \quad \text{and} \quad G(z, r_0) \equiv R \frac{C}{B} (1-z)^4. \quad (67)$$

In terms of z , notice that $R(r)$ reads

$$R(r) = D_0 r_0 z + \left[\frac{r_0}{2} \left(\frac{C_0''}{C_0} - \frac{A_0''}{A_0} \right) + \left(1 - \frac{A_0' r_0}{A_0} \right) D_0 \right] r_0 z^2 + \mathcal{O}(z^3) + \dots \quad (68)$$

Expanding $G(z, r_0)$ in terms of z , we have:

$$G(z, r_0) = \sum_{n=1}^{\infty} c_n(r_0) z^n, \quad (69)$$

where $c_1(r)$ and $c_2(r)$ are

$$c_1(r_0) = \frac{C_0 D_0 r_0}{B_0}, \quad (70)$$

and

$$c_2(r_0) = \frac{C_0 r_0}{B_0} \left\{ D_0 \left[\left(D_0 - \frac{B_0'}{B_0} \right) r_0 - 3 \right] + \frac{r_0}{2} \left(\frac{C_0''}{C_0} - \frac{A_0''}{A_0} \right) \right\}. \quad (71)$$

Moreover, by considering the strong deflection limit, it turns out that

$$c_1(r_m) = 0, \quad \text{and} \quad c_2(r_m) = \frac{C_m r_m^2}{2B_m} D'_m, \quad \text{with} \quad D'_m = \frac{C''}{C_m} - \frac{A''}{A_m}. \quad (72)$$

Here, $G(z, r_0)$ possess a shorter notation, as shown below:

$$G_m(z) = c_2(r_m)z^2 + \mathcal{O}(z^3). \quad (73)$$

This shows that the main divergence of $f(z, r_0)$ happens at the order of z^{-1} , causing a logarithmic divergence in the integral $I(r_0)$ as r_0 gets close to r_m . To manage this divergence, we split the integral $I(r_0)$ into two parts: a divergent part, $I_D(r_0)$, and a regular part, $I_R(r_0)$. In this sense, the divergent part $I_D(r_0)$ is properly written as:

$$I_D(r_0) \equiv \int_0^1 f_D(z, r_0) dz, \quad \text{with} \quad f_D(z, r_0) \equiv \frac{2r_0}{\sqrt{c_1(r_0)z + c_2(r_0)z^2}}. \quad (74)$$

After integrating, we obtain

$$I_D(r_0) = \frac{4r_0}{\sqrt{c_2(r_0)}} \ln \left[\frac{\sqrt{c_2(r_0)} + \sqrt{c_1(r_0) + c_2(r_0)}}{\sqrt{c_1(r_0)}} \right]. \quad (75)$$

Considering the expansion of $c_1(r_0)$ and $b(r_0)$ around $r_0 - r_m$

$$c_1(r_0) = \frac{C_m r_m D'_m}{B_m} (r_0 - r_m) + \mathcal{O}((r_0 - r_m)^2), \quad (76)$$

and

$$b(r_0) = b_c(r_m) + \frac{1}{4} \sqrt{\frac{C_m}{A_m}} D'_m (r_0 - r_m)^2 + \mathcal{O}((r_0 - r_m)^3), \quad (77)$$

leading to the following in the strong deflection limit

$$\lim_{r_0 \rightarrow r_m} c_1(r_0) = \lim_{b \rightarrow b_c} \frac{2C_m r_m \sqrt{D'_m}}{B_m} \left(\frac{b}{b_c} - 1 \right)^{1/2}. \quad (78)$$

Thereby, $I_D(b)$ is

$$I_D(b) = -\frac{r_m}{\sqrt{c_2(r_m)}} \ln \left[\frac{b}{b_c} - 1 \right] + \frac{r_m}{\sqrt{c_2(r_m)}} \ln [r^2 D'_m] + \mathcal{O}[(b - b_c) \ln(b - b_c)]. \quad (79)$$

Meanwhile, we define $I_R(b)$ as

$$I_R(b) = \int_1^0 f_R(z, b_c) dz + \mathcal{O}[(b - b_c) \ln(b - b_c)]. \quad (80)$$

Here, let f_R be defined as $f_R = f(z, r_0) - f_D(z, r_0)$. In the strong deflection limit, the deflection angle is given by

$$a(b) = -\tilde{a} \ln \left[\frac{b}{b_c} - 1 \right] + \tilde{b} + \mathcal{O}[(b - b_c) \ln(b - b_c)], \quad (81)$$

in which

$$\tilde{a} = \sqrt{\frac{2B_m A_m}{C''_m A_m - C_m A''_m}}, \quad \text{and} \quad \tilde{b} = \tilde{a} \ln \left[r_m^2 \left(\frac{C''}{C_m} - \frac{A''}{A_m} \right) \right] + I_R(r_m) - \pi. \quad (82)$$

A. Gravitational lensing of a non-commutative black hole

After all the methodology presented above, let us apply it to our metric under consideration in Eq. (4). Then, we have

$$b_c = \frac{1}{2} \sqrt{\frac{\left(\sqrt{M(9\sqrt{\pi}M - 64\sqrt{\Theta})} + 3\sqrt[4]{\pi}M\right)^4}{6\pi M^2 - 32\sqrt{\pi}\sqrt{\Theta}M + 2\pi^{3/4}M\sqrt{M(9\sqrt{\pi}M - 64\sqrt{\Theta})}}}. \quad (83)$$

Also, \tilde{a} and \tilde{b} can be expressed as

$$\tilde{a} = \sqrt[4]{\pi} \sqrt{\frac{1}{\sqrt{\pi} - \frac{64\sqrt{\Theta}M}{\left(\frac{\sqrt{M(9\sqrt{\pi}M - 64\sqrt{\Theta})}}{\sqrt[4]{\pi}} + 3M\right)^2}}}, \quad (84)$$

In this sense, we can write

$$\tilde{b} = \sqrt[4]{\pi} \sqrt{\frac{1}{\sqrt{\pi} - \frac{64\sqrt{\Theta}M}{\left(\frac{\sqrt{M(9\sqrt{\pi}M - 64\sqrt{\Theta})}}{\sqrt[4]{\pi}} + 3M\right)^2}} \ln\left(\frac{8}{\frac{\sqrt[4]{\pi}M}{\sqrt{M(9\sqrt{\pi}M - 64\sqrt{\Theta})}} + 1}\right) + I_R(r_m) - \pi. \quad (85)$$

In contrast with what happens in the Schwarzschild case, notice that the contribution to the parameter \tilde{a} is fundamentally due to the feature coming from the non-commutativity. In addition, $I_R(r_m)$ can be calculated as

$$\begin{aligned} I_R(r_m) &= \int_0^1 dz \left\{ \sqrt{2} \left(\sqrt{M(9\sqrt{\pi}M - 64\sqrt{\Theta})} + 3\sqrt[4]{\pi}M \right) \right. \\ &\quad \times \left[-\frac{1}{\sqrt{Mz^2(-64\sqrt{\Theta} + 3\sqrt[4]{\pi}\sqrt{M(9\sqrt{\pi}M - 64\sqrt{\Theta})} + 9\sqrt{\pi}M)}} \right. \\ &\quad \left. \left. + \frac{1}{\sqrt{Mz^2\left(\sqrt[4]{\pi}(3-2z)\sqrt{M(9\sqrt{\pi}M - 64\sqrt{\Theta})} + 3\sqrt{\pi}M(3-2z) - 16\sqrt{\Theta}(z-2)^2\right)}} \right] \right\} \\ &= 0.82439. \end{aligned} \quad (86)$$

Here, we have evaluated $I_R(r_m)$ numerically, considering $M = 2$ and $\Theta = 0.1$. In this manner, the deflection angle

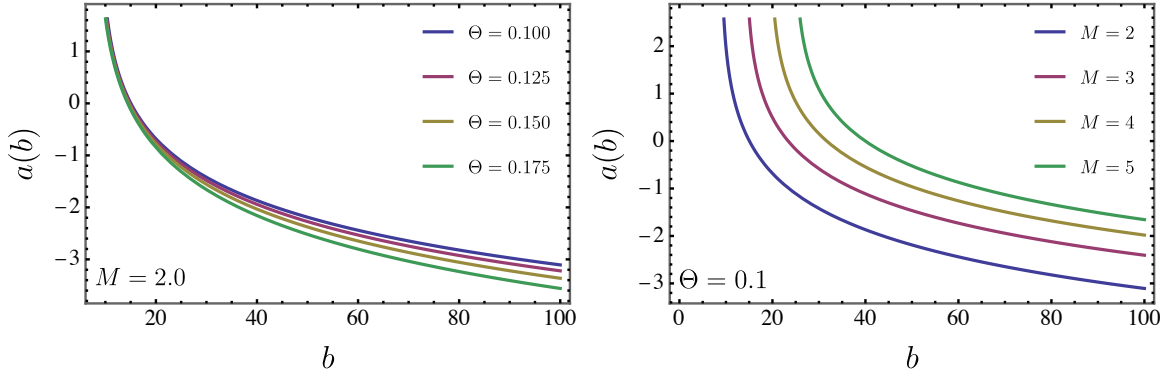


Figure 13: The deflection angle as a function of b for different values of Θ and M .

shown in Eq. (81) reads

$$\begin{aligned}
a(b) = & -\sqrt[4]{\pi} \frac{1}{\sqrt{\sqrt{\pi} - \frac{64\sqrt{\Theta}M}{\left(\frac{\sqrt{M(9\sqrt{\pi}M-64\sqrt{\Theta})}}{\sqrt[4]{\pi}} + 3M\right)^2}}} \ln \left[\frac{b}{\frac{1}{2} \sqrt{\frac{\left(\sqrt{M(9\sqrt{\pi}M-64\sqrt{\Theta})} + 3\sqrt[4]{\pi}M\right)^4}{6\pi M^2 - 32\sqrt{\pi}\sqrt{\Theta}M + 2\pi^{3/4}M\sqrt{M(9\sqrt{\pi}M-64\sqrt{\Theta})}}} - 1} \right] \\
& + \sqrt[4]{\pi} \frac{1}{\sqrt{\sqrt{\pi} - \frac{64\sqrt{\Theta}M}{\left(\frac{\sqrt{M(9\sqrt{\pi}M-64\sqrt{\Theta})}}{\sqrt[4]{\pi}} + 3M\right)^2}}} \ln \left(\frac{8}{\frac{\sqrt[4]{\pi}M}{\sqrt{M(9\sqrt{\pi}M-64\sqrt{\Theta})}} + 1} \right) + 0.82439 - \pi \\
& + \mathcal{O} \left\{ \left(b - \frac{1}{2} \sqrt{\frac{\left(\sqrt{M(9\sqrt{\pi}M-64\sqrt{\Theta})} + 3\sqrt[4]{\pi}M\right)^4}{6\pi M^2 - 32\sqrt{\pi}\sqrt{\Theta}M + 2\pi^{3/4}M\sqrt{M(9\sqrt{\pi}M-64\sqrt{\Theta})}}} \right) \right. \\
& \left. \times \ln \left[b - \frac{1}{2} \sqrt{\frac{\left(\sqrt{M(9\sqrt{\pi}M-64\sqrt{\Theta})} + 3\sqrt[4]{\pi}M\right)^4}{6\pi M^2 - 32\sqrt{\pi}\sqrt{\Theta}M + 2\pi^{3/4}M\sqrt{M(9\sqrt{\pi}M-64\sqrt{\Theta})}}} \right] \right\}. \tag{87}
\end{aligned}$$

To enhance clarity for the reader, we present Fig. 13, illustrating the deflection angle as a function of b across various system configurations.

VII. CONCLUSION

Our investigation was centered on exploring the gravitational signatures of a non-commutative black hole. Specifically, we selected a distinct mass distribution, described by the mathematical expression $\rho_{\Theta}(r) = M\sqrt{\Theta}/\pi^{3/2}(r^2 + \pi\Theta)^2$, to derive the corresponding black hole solution. This theory revealed the presence of two horizons: an event horizon and a Cauchy horizon.

In addition, we calculated the Hawking temperature using two different methodologies: the topological method and surface gravity analysis. Additionally, we examined entropy and heat capacity to investigate further the thermodynamic properties of the system. Our comparisons extended to contrasting thermal quantities with those of the usual Schwarzschild black hole and its modified counterpart within non-commutative gauge theory [9].

In our study of the evaporation process, we initially determined the remnant mass by considering the black hole's final state, where $T_{\Theta} \rightarrow 0$. Subsequently, we derived an analytical expression for the time evaporation up to a *grey-*

body factor. Furthermore, we estimated the black hole lifetime for specific initial and final masses, yielding $t_{evap} = \frac{1}{\xi} (2.51807 \times 10^7)$. Furthermore, we computed the emission rate, taking into account the high-energy absorption cross-section for observers at infinity. Also, to address quasinormal modes, we analyzed tensorial perturbations using the 6th WKB approximation. The weak and strong deflection limits were computed by employing the Gauss-Bonnet theorem and Tsukamoto methods, respectively.

In the future, we aim to explore the gravitational lensing of black holes within a non-commutative gauge theory, which will expand our comprehension of these celestial phenomena.

Appendix

Here, we present the analytical expression for the evaporation time t_{evap} up to a *grey-body* factor:

$$\begin{aligned}
t_{\text{evap}} = \frac{8\pi^{7/2}}{\xi} \left\{ \frac{8}{243\pi\delta M (\sqrt{\pi}\delta M - 8\sqrt{\Theta})} \right. & \left[243\pi^2\delta M^5 + 243\pi^{7/4}\delta M^4 \sqrt{\delta M (\sqrt{\pi}\delta M - 8\sqrt{\Theta})} \right. \\
+ 81\pi^{7/4}\delta M^4 \sqrt{\delta M (9\sqrt{\pi}\delta M - 64\sqrt{\Theta})} & + 81\pi^{3/2}\delta M^3 \sqrt{\delta M (9\sqrt{\pi}\delta M - 64\sqrt{\Theta})} \sqrt{\delta M (\sqrt{\pi}\delta M - 8\sqrt{\Theta})} \\
+ 180\pi^{5/4}\delta M^3 \sqrt{\Theta} \sqrt{\delta M (9\sqrt{\pi}\delta M - 64\sqrt{\Theta})} & - 972\pi^{3/2}\delta M^4 \sqrt{\Theta} \\
+ 504\pi\delta M^2 \sqrt{\Theta} \sqrt{\delta M (9\sqrt{\pi}\delta M - 64\sqrt{\Theta})} & \sqrt{\delta M (\sqrt{\pi}\delta M - 8\sqrt{\Theta})} + 13608\pi\delta M^3 \Theta \\
15552\pi^{3/4}\delta M^2 \Theta \sqrt{\delta M (\sqrt{\pi}\delta M - 8\sqrt{\Theta})} & + 5880\pi^{3/4}\delta M^2 \Theta \sqrt{\delta M (9\sqrt{\pi}\delta M - 64\sqrt{\Theta})} \\
+ 8544\sqrt{\pi}\delta M \Theta \sqrt{\delta M (9\sqrt{\pi}\delta M - 64\sqrt{\Theta})} & \sqrt{\delta M (\sqrt{\pi}\delta M - 8\sqrt{\Theta})} - 171072\sqrt{\pi}\delta M^2 \Theta^{3/2} \\
- 373248\sqrt[4]{\pi}\delta M \Theta^{3/2} \sqrt{\delta M (\sqrt{\pi}\delta M - 8\sqrt{\Theta})} & - 115584\sqrt[4]{\pi}\delta M \Theta^{3/2} \sqrt{\delta M (9\sqrt{\pi}\delta M - 64\sqrt{\Theta})} \\
- 266496\Theta^{3/2} \sqrt{\delta M (9\sqrt{\pi}\delta M - 64\sqrt{\Theta})} & \sqrt{\delta M (\sqrt{\pi}\delta M - 8\sqrt{\Theta})} - 124416\delta M \Theta^2 \\
1813504\delta M \Theta^2 \ln(\delta M) - 226688\sqrt{\pi}\delta M^2 \Theta^{3/2} \ln(\delta M) & \\
- 217728\sqrt{\pi}\delta M^2 \Theta^{3/2} \ln \left(\sqrt[4]{\pi} \sqrt{\delta M (9\sqrt{\pi}\delta M - 64\sqrt{\Theta})} & + 5\sqrt{\pi}\delta M - 32\sqrt{\Theta} \right) \\
+ 1741824\delta M \Theta^2 \ln \left(\sqrt[4]{\pi} \sqrt{\delta M (9\sqrt{\pi}\delta M - 64\sqrt{\Theta})} & + 5\sqrt{\pi}\delta M - 32\sqrt{\Theta} \right) \\
+ 226688\sqrt{\pi}\delta M^2 \Theta^{3/2} \ln \left(3\sqrt[4]{\pi} \sqrt{\delta M (9\sqrt{\pi}\delta M - 64\sqrt{\Theta})} & + 9\sqrt{\pi}\delta M - 32\sqrt{\Theta} \right) \\
- 1813504\delta M \Theta^2 \ln \left(3\sqrt[4]{\pi} \sqrt{\delta M (9\sqrt{\pi}\delta M - 64\sqrt{\Theta})} & + 9\sqrt{\pi}\delta M - 32\sqrt{\Theta} \right) \\
+ 404352\sqrt{\pi}\delta M^2 \Theta^{3/2} \ln \left(\sqrt{\pi}\delta M - 8\sqrt{\Theta} \right) & - 3234816\delta M \Theta^2 \ln \left(\sqrt{\pi}\delta M - 8\sqrt{\Theta} \right) \\
+ 186624\sqrt{\pi}\delta M^2 \Theta^{3/2} \ln \left(\sqrt[4]{\pi} \sqrt{M (\sqrt{\pi}\delta M - 8\sqrt{\Theta})} & + \sqrt{\pi}\delta M - 4\sqrt{\Theta} \right) \\
- 1492992\delta M \Theta^2 \ln \left(\sqrt[4]{\pi} \sqrt{\delta M (\sqrt{\pi}\delta M - 8\sqrt{\Theta})} & + \sqrt{\pi}\delta M - 4\sqrt{\Theta} \right) \\
+ 226688\sqrt{\pi}\delta M^2 \Theta^{3/2} \ln \left(9\sqrt{\pi}\delta M^2 - 68\delta M \sqrt{\Theta} & + 3\sqrt{\delta M (\sqrt{\pi}\delta M - 8\sqrt{\Theta})} \sqrt{\delta M (9\sqrt{\pi}\delta M - 64\sqrt{\Theta})} \right) \\
- 1813504\delta M \Theta^2 \ln \left(9\sqrt{\pi}\delta M^2 - 68\delta M \sqrt{\Theta} & + 3\sqrt{\delta M (\sqrt{\pi}\delta M - 8\sqrt{\Theta})} \sqrt{\delta M (9\sqrt{\pi}\delta M - 64\sqrt{\Theta})} \right) \left. \right\}.
\end{aligned} \tag{88}$$

It is important to mention that the notation of δM means the application of the limits of integration, i.e., $\delta M = M_{\text{rem}} - M_i$.

Acknowledgments

The authors would like to thank the Conselho Nacional de Desenvolvimento Científico e Tecnológico (CNPq) for financial support. P. J. Porfírio would like to acknowledge the Brazilian agency CNPq, grant No. 307628/2022-1. The work by A. Yu. Petrov has been partially supported by the CNPq project No. 303777/2023-0. Moreover, A. A. Araújo Filho is supported by Conselho Nacional de Desenvolvimento Científico e Tecnológico (CNPq) and Fundação de Apoio à Pesquisa do Estado da Paraíba (FAPESQ), project No. 150891/2023-7. A. Ô. would like to acknowledge the contribution of the COST Action CA21106 - COSMIC WISPerS in the Dark Universe: Theory, astrophysics and experiments (CosmicWISPerS) and the COST Action CA22113 - Fundamental challenges in theoretical physics (THEORY-CHALLENGES). We also thank TUBITAK and SCOAP3 for their support.

-
- [1] R. J. Szabo, “Symmetry, gravity and noncommutativity,” *Classical and Quantum Gravity*, vol. 23, no. 22, p. R199, 2006.
 - [2] R. J. Szabo, “Quantum field theory on noncommutative spaces,” *Physics Reports*, vol. 378, no. 4, pp. 207–299, 2003.
 - [3] N. Seiberg and E. Witten, “String theory and noncommutative geometry,” *Journal of High Energy Physics*, vol. 1999, no. 09, p. 032, 1999.
 - [4] A. F. Ferrari, H. O. Girotti, M. Gomes, A. Y. Petrov, A. Ribeiro, and A. Da Silva, “On the finiteness of noncommutative supersymmetric qed3 in the covariant superfield formulation,” *Physics Letters B*, vol. 577, no. 1-2, pp. 83–92, 2003.
 - [5] A. F. Ferrari, H. O. Girotti, M. Gomes, A. Y. Petrov, A. Ribeiro, V. O. Rivelles, and A. Da Silva, “Superfield covariant analysis of the divergence structure of noncommutative supersymmetric qed 4,” *Physical Review D*, vol. 69, no. 2, p. 025008, 2004.
 - [6] A. F. Ferrari, H. O. Girotti, M. Gomes, A. Y. Petrov, A. Ribeiro, V. O. Rivelles, and A. da Silva, “Towards a consistent noncommutative supersymmetric yang-mills theory: Superfield covariant analysis,” *Physical Review D*, vol. 70, no. 8, p. 085012, 2004.
 - [7] A. H. Chamseddine, “Deforming einstein’s gravity,” *Physics Letters B*, vol. 504, no. 1-2, pp. 33–37, 2001.
 - [8] Y. S. Myung, Y.-W. Kim, and Y.-J. Park, “Thermodynamics and evaporation of the noncommutative black hole,” *Journal of High Energy Physics*, vol. 2007, no. 02, p. 012, 2007.
 - [9] A. A. Araújo Filho, S. Zare, P. J. Porfírio, J. Kříž, and H. Hassanabadi, “Thermodynamics and evaporation of a modified schwarzschild black hole in a non-commutative gauge theory,” *Physics Letters B*, vol. 838, p. 137744, 2023.
 - [10] R. Banerjee, B. R. Majhi, and S. Samanta, “Noncommutative black hole thermodynamics,” *Physical Review D*, vol. 77, no. 12, p. 124035, 2008.
 - [11] J. Lopez-Dominguez, O. Obregon, M. Sabido, and C. Ramirez, “Towards noncommutative quantum black holes,” *Physical Review D*, vol. 74, no. 8, p. 084024, 2006.
 - [12] M. Sharif and W. Javed, “Thermodynamics of a bardeen black hole in noncommutative space,” *Canadian Journal of Physics*, vol. 89, no. 10, pp. 1027–1033, 2011.
 - [13] K. Nozari and B. Fazlpour, “Reissner-nordstr\”{o} m black hole thermodynamics in noncommutative spaces,” *arXiv preprint gr-qc/0608077*, 2006.
 - [14] K. Nozari and B. Fazlpour, “Thermodynamics of noncommutative schwarzschild black hole,” *Modern Physics Letters A*, vol. 22, no. 38, pp. 2917–2930, 2007.
 - [15] P. Nicolini, A. Smailagic, and E. Spallucci, “Noncommutative geometry inspired schwarzschild black hole,” *Physics Letters B*, vol. 632, no. 4, pp. 547–551, 2006.
 - [16] N. Heidari, H. Hassanabadi, A. A. P. Araújo Filho, and J. Kriz, “Exploring non-commutativity as a perturbation in the schwarzschild black hole: quasinormal modes, scattering, and shadows,” *The European Physical Journal C*, vol. 84, p. 566, 2024.
 - [17] W. Unno, Y. Osaki, H. Ando, and H. Shibahashi, “Nonradial oscillations of stars,” *Tokyo: University of Tokyo Press*, 1979.
 - [18] H. Kjeldsen and T. R. Bedding, “Amplitudes of stellar oscillations: the implications for asteroseismology,” *arXiv preprint astro-ph/9403015*, 1994.
 - [19] W. Dziembowski and P. R. Goode, “Effects of differential rotation on stellar oscillations—a second-order theory,” *The Astrophysical Journal*, vol. 394, pp. 670–687, 1992.
 - [20] F. Pretorius, “Evolution of binary black-hole spacetimes,” *Physical review letters*, vol. 95, no. 12, p. 121101, 2005.
 - [21] J. R. Hurley, C. A. Tout, and O. R. Pols, “Evolution of binary stars and the effect of tides on binary populations,” *Monthly Notices of the Royal Astronomical Society*, vol. 329, no. 4, pp. 897–928, 2002.
 - [22] K. Yakut and P. P. Eggleton, “Evolution of close binary systems,” *The Astrophysical Journal*, vol. 629, no. 2, p. 1055, 2005.
 - [23] E. v. d. Heuvel, “Compact stars and the evolution of binary systems,” in *Fluid Flows To Black Holes: A Tribute to S Chandrasekhar on His Birth Centenary*, pp. 55–73, World Scientific, 2011.
 - [24] K. Riles, “Recent searches for continuous gravitational waves,” *Modern Physics Letters A*, vol. 32, no. 39, p. 1730035, 2017.
 - [25] Á. Rincón and V. Santos, “Greybody factor and quasinormal modes of regular black holes,” *The European Physical*

- Journal C*, vol. 80, no. 10, pp. 1–7, 2020.
- [26] V. Santos, R. V. Maluf, and C. A. S. Almeida, “Quasinormal frequencies of self-dual black holes,” *Physical Review D*, vol. 93, no. 8, p. 084047, 2016.
- [27] R. Oliveira, D. Dantas, V. Santos, and C. Almeida, “Quasinormal modes of bumblebee wormhole,” *Classical and Quantum Gravity*, vol. 36, no. 10, p. 105013, 2019.
- [28] E. Berti, V. Cardoso, and A. O. Starinets, “Quasinormal modes of black holes and black branes,” *Classical and Quantum Gravity*, vol. 26, no. 16, p. 163001, 2009.
- [29] G. T. Horowitz and V. E. Hubeny, “Quasinormal modes of ads black holes and the approach to thermal equilibrium,” *Physical Review D*, vol. 62, no. 2, p. 024027, 2000.
- [30] H.-P. Nollert, “Quasinormal modes: the characteristics of black holes and neutron stars,” *Classical and Quantum Gravity*, vol. 16, no. 12, p. R159, 1999.
- [31] V. Ferrari and B. Mashhoon, “New approach to the quasinormal modes of a black hole,” *Physical Review D*, vol. 30, no. 2, p. 295, 1984.
- [32] K. Jusufi, B. Cuadros-Melgar, G. Leon, A. Jawad, *et al.*, “Charged black holes with yukawa potential,” *arXiv preprint arXiv:2401.15211*, 2024.
- [33] N. Heidari, J. Reis, H. Hassanabadi, *et al.*, “The impact of an antisymmetric tensor on charged black holes: evaporation process, geodesics, deflection angle, scattering effects and quasinormal modes,” *arXiv preprint arXiv:2404.10721*, 2024.
- [34] K. D. Kokkotas and B. G. Schmidt, “Quasi-normal modes of stars and black holes,” *Living Reviews in Relativity*, vol. 2, no. 1, pp. 1–72, 1999.
- [35] A. A. Araújo Filho, K. Jusufi, B. Cuadros-Melgar, and G. Leon, “Dark matter signatures of black holes with yukawa potential,” *Physics of the Dark Universe*, p. 101500, 2024.
- [36] L. London, D. Shoemaker, and J. Healy, “Modeling ringdown: Beyond the fundamental quasinormal modes,” *Physical Review D*, vol. 90, no. 12, p. 124032, 2014.
- [37] M. Maggiore, “Physical interpretation of the spectrum of black hole quasinormal modes,” *Physical Review Letters*, vol. 100, no. 14, p. 141301, 2008.
- [38] A. Flachi and J. P. Lemos, “Quasinormal modes of regular black holes,” *Physical Review D*, vol. 87, no. 2, p. 024034, 2013.
- [39] A. Övgün, I. Sakalli, and J. Saavedra, “Quasinormal modes of a schwarzschild black hole immersed in an electromagnetic universe,” *Chinese Physics C*, vol. 42, no. 10, p. 105102, 2018.
- [40] J. L. Blázquez-Salcedo, X. Y. Chew, and J. Kunz, “Scalar and axial quasinormal modes of massive static phantom wormholes,” *Physical Review D*, vol. 98, no. 4, p. 044035, 2018.
- [41] P. D. Roy, S. Aneesh, and S. Kar, “Revisiting a family of wormholes: geometry, matter, scalar quasinormal modes and echoes,” *The European Physical Journal C*, vol. 80, no. 9, pp. 1–17, 2020.
- [42] R. Konoplya and A. Zhidenko, “Quasinormal modes of black holes: From astrophysics to string theory,” *Reviews of Modern Physics*, vol. 83, no. 3, p. 793, 2011.
- [43] J. Y. Kim, C. O. Lee, and M.-I. Park, “Quasi-normal modes of a natural ads wormhole in einstein–born–infeld gravity,” *The European Physical Journal C*, vol. 78, no. 12, pp. 1–15, 2018.
- [44] C. O. Lee, J. Y. Kim, and M.-I. Park, “Quasi-normal modes and stability of einstein–born–infeld black holes in de sitter space,” *The European Physical Journal C*, vol. 80, no. 8, pp. 1–21, 2020.
- [45] A. Jawad, S. Chaudhary, M. Yasir, A. Övgün, and İ. Sakalli, “Quasinormal modes of extended gravity black holes through higher order wkb method,” *International Journal of Geometric Methods in Modern Physics*, p. 2350129, 2023.
- [46] A. A. Araújo Filho, J. A. A. S. Reis, and H. Hassanabadi, “Exploring antisymmetric tensor effects on black hole shadows and quasinormal frequencies,” *Journal of Cosmology and Astroparticle Physics*, vol. 2024, no. 05, p. 029, 2024.
- [47] R. Maluf, V. Santos, W. Cruz, and C. Almeida, “Matter-gravity scattering in the presence of spontaneous lorentz violation,” *Physical Review D*, vol. 88, no. 2, p. 025005, 2013.
- [48] R. Maluf, C. Almeida, R. Casana, and M. Ferreira Jr, “Einstein-hilbert graviton modes modified by the lorentz-violating bumblebee field,” *Physical Review D*, vol. 90, no. 2, p. 025007, 2014.
- [49] M. Okyay and A. Övgün, “Nonlinear electrodynamics effects on the black hole shadow, deflection angle, quasinormal modes and greybody factors,” *Journal of Cosmology and Astroparticle Physics*, vol. 2022, no. 01, p. 009, 2022.
- [50] Y. Zhao, X. Ren, A. Ilyas, E. N. Saridakis, and Y.-F. Cai, “Quasinormal modes of black holes in f (t) gravity,” *Journal of Cosmology and Astroparticle Physics*, vol. 2022, no. 10, p. 087, 2022.
- [51] S. Boudet, F. Bombacigno, G. J. Olmo, and P. J. Porfirio, “Quasinormal modes of schwarzschild black holes in projective invariant chern-simons modified gravity,” *Journal of Cosmology and Astroparticle Physics*, vol. 2022, no. 05, p. 032, 2022.
- [52] M. Cadoni, M. Oi, and A. P. Sanna, “Quasi-normal modes and microscopic description of 2d black holes,” *Journal of High Energy Physics*, vol. 2022, no. 1, pp. 1–23, 2022.
- [53] L. Hui, D. Kabat, and S. S. Wong, “Quasinormal modes, echoes and the causal structure of the green’s function,” *Journal of Cosmology and Astroparticle Physics*, vol. 2019, no. 12, p. 020, 2019.
- [54] A. A. Araújo Filho, H. Hassanabadi, N. Heidari, J. Kríž, and S. Zare, “Gravitational traces of bumblebee gravity in metric-affine formalism,” *Class. Quant. Grav.*, vol. 41, p. 055003, 2024.
- [55] N. Heidari, H. Hassanabadi, A. A. Araújo Filho, J. Kríž, S. Zare, and P. J. Porfirio, “Gravitational signatures of a non-commutative stable black hole,” *Physics of the Dark Universe*, vol. 43, p. 101382, 2023.
- [56] A. A. Araújo Filho, “Analysis of a regular black hole in verlinde’s gravity,” *Classical and Quantum Gravity*, vol. 41, no. 1, p. 015003, 2023.
- [57] A. A. Araújo Filho, “Implications of a simpson–visser solution in verlinde’s framework,” *The European Physical Journal*

- C*, vol. 84, no. 1, pp. 1–22, 2024.
- [58] D. J. Gogoi, A. Övgün, and M. Koussour, “Quasinormal modes of black holes in $f(q)$ gravity,” *arXiv preprint arXiv:2303.07424*, 2023.
- [59] D. Liu, Y. Yang, A. Övgün, Z.-W. Long, and Z. Xu, “The quasinormal modes and greybody bounds of rotating black holes in a dark matter halo,” *arXiv preprint arXiv:2204.11563*, 2022.
- [60] Y. Yang, D. Liu, A. Övgün, Z.-W. Long, and Z. Xu, “Probing hairy black holes caused by gravitational decoupling using quasinormal modes and greybody bounds,” *Physical Review D*, vol. 107, no. 6, p. 064042, 2023.
- [61] D. J. Gogoi, A. Övgün, and D. Demir, “Quasinormal modes and greybody factors of symmergent black hole,” *Phys. Dark Univ.*, vol. 42, p. 101314, 2023.
- [62] G. Lambiase, R. C. Pantig, D. J. Gogoi, and A. Övgün, “Investigating the connection between generalized uncertainty principle and asymptotically safe gravity in black hole signatures through shadow and quasinormal modes,” *arXiv preprint arXiv:2304.00183*, 2023.
- [63] S. Fernando, “Quasinormal modes of dilaton-de Sitter black holes: scalar perturbations,” *Gen. Rel. Grav.*, vol. 48, no. 3, p. 24, 2016.
- [64] S. Fernando and J. Correa, “Quasinormal Modes of Bardeen Black Hole: Scalar Perturbations,” *Phys. Rev. D*, vol. 86, p. 064039, 2012.
- [65] R. G. Daghigh and M. D. Green, “Highly Real, Highly Damped, and Other Asymptotic Quasinormal Modes of Schwarzschild-Anti De Sitter Black Holes,” *Class. Quant. Grav.*, vol. 26, p. 125017, 2009.
- [66] R. G. Daghigh, M. D. Green, and J. C. Morey, “Significance of Black Hole Quasinormal Modes: A Closer Look,” *Phys. Rev. D*, vol. 101, no. 10, p. 104009, 2020.
- [67] R. G. Daghigh and G. Kunstatter, “Highly damped quasinormal modes of generic single horizon black holes,” *Class. Quant. Grav.*, vol. 22, pp. 4113–4128, 2005.
- [68] R. G. Daghigh, M. D. Green, J. C. Morey, and G. Kunstatter, “Scalar Perturbations of a Single-Horizon Regular Black Hole,” *Phys. Rev. D*, vol. 102, no. 10, p. 104040, 2020.
- [69] R. G. Daghigh, M. D. Green, and G. Kunstatter, “Scalar Perturbations and Stability of a Loop Quantum Corrected Kruskal Black Hole,” *Phys. Rev. D*, vol. 103, no. 8, p. 084031, 2021.
- [70] R. G. Daghigh, M. D. Green, and J. C. Morey, “Calculating quasinormal modes of Schwarzschild anti-de Sitter black holes using the continued fraction method,” *Phys. Rev. D*, vol. 107, no. 2, p. 024023, 2023.
- [71] D. J. Gogoi, A. Övgün, and M. Koussour, “Quasinormal modes of black holes in $f(Q)$ gravity,” *Eur. Phys. J. C*, vol. 83, no. 8, p. 700, 2023.
- [72] Y. Yang, D. Liu, A. Övgün, Z.-W. Long, and Z. Xu, “Probing hairy black holes caused by gravitational decoupling using quasinormal modes and greybody bounds,” *Phys. Rev. D*, vol. 107, no. 6, p. 064042, 2023.
- [73] B. Abbott, S. Jawahar, N. Lockerbie, and K. Tokmakov, “Ligo scientific collaboration and virgo collaboration (2016) directly comparing gw150914 with numerical solutions of einstein’s equations for binary black hole coalescence,” *Phys. Rev. D*, vol. 94, p. 064035, 2016.
- [74] B. P. Abbott, R. Abbott, T. Abbott, M. Abernathy, F. Acernese, K. Ackley, C. Adams, T. Adams, P. Addesso, R. Adhikari, *et al.*, “Gw151226: observation of gravitational waves from a 22-solar-mass binary black hole coalescence,” *Phys. Rev. Lett.*, vol. 116, no. 24, p. 241103, 2016.
- [75] B. P. Abbott, R. Abbott, T. Abbott, F. Acernese, K. Ackley, C. Adams, T. Adams, P. Addesso, R. X. Adhikari, V. B. Adya, *et al.*, “Gw170814: a three-detector observation of gravitational waves from a binary black hole coalescence,” *Phys. Rev. Lett.*, vol. 119, no. 14, p. 141101, 2017.
- [76] O. Contigiani, “Lensing efficiency for gravitational wave mergers,” *Monthly Notices of the Royal Astronomical Society*, vol. 492, no. 3, pp. 3359–3363, 2020.
- [77] S. Mukherjee, B. D. Wandelt, and J. Silk, “Probing the theory of gravity with gravitational lensing of gravitational waves and galaxy surveys,” *Monthly Notices of the Royal Astronomical Society*, vol. 494, no. 2, pp. 1956–1970, 2020.
- [78] S. Vagnozzi, R. Roy, Y.-D. Tsai, L. Visinelli, M. Afrin, A. Allahyari, P. Bambhaniya, D. Dey, S. G. Ghosh, P. S. Joshi, *et al.*, “Horizon-scale tests of gravity theories and fundamental physics from the event horizon telescope image of sagittarius a,” *Classical and Quantum Gravity*, 2022.
- [79] C. G. Darwin, “The gravity field of a particle,” *Proceedings of the Royal Society of London. Series A. Mathematical and Physical Sciences*, vol. 249, no. 1257, pp. 180–194, 1959.
- [80] R. d. Atkinson, “On light tracks near a very massive star,” *Astronomical Journal*, Vol. 70, p. 517, vol. 70, p. 517, 1965.
- [81] F. Eisenhauer, R. Genzel, T. Alexander, R. Abuter, T. Paumard, T. Ott, A. Gilbert, S. Gillessen, M. Horrobin, S. Trippe, *et al.*, “Sinfoni in the galactic center: young stars and infrared flares in the central light-month,” *The Astrophysical Journal*, vol. 628, no. 1, p. 246, 2005.
- [82] E. H. T. Collaboration *et al.*, “First m87 event horizon telescope results. iv. imaging the central supermassive black hole,” *arXiv preprint arXiv:1906.11241*, 2019.
- [83] K. Akiyama, A. Alberdi, W. Alef, K. Asada, R. Azulay, A.-K. Baczkó, D. Ball, M. Baloković, J. Barrett, D. Bintley, *et al.*, “First m87 event horizon telescope results. ii. array and instrumentation,” *The Astrophysical Journal Letters*, vol. 875, no. 1, p. L2, 2019.
- [84] K. Akiyama, A. Alberdi, W. Alef, K. Asada, R. Azulay, A.-K. Baczkó, D. Ball, M. Baloković, J. Barrett, D. Bintley, *et al.*, “First m87 event horizon telescope results. v. physical origin of the asymmetric ring,” *The Astrophysical Journal Letters*, vol. 875, no. 1, p. L5, 2019.
- [85] E. H. T. Collaboration *et al.*, “First m87 event horizon telescope results. iv. imaging the central supermassive black hole,” *arXiv preprint arXiv:1906.11241*, 2019.

- [86] K. Akiyama, A. Alberdi, W. Alef, K. Asada, R. Azulay, A.-K. Bacsko, D. Ball, M. Baloković, J. Barrett, D. Bintley, *et al.*, “First m87 event horizon telescope results. v. physical origin of the asymmetric ring,” *The Astrophysical Journal Letters*, vol. 875, no. 1, p. L5, 2019.
- [87] D. Ball, C.-K. Chan, P. Christian, B. T. Jannuzi, J. Kim, D. P. Marrone, L. Medeiros, F. Ozel, D. Psaltis, M. Rose, *et al.*, “First m87 event horizon telescope results. vi. the shadow and mass of the central black hole,” 2019.
- [88] R. C. Pantig, A. Övgün, and D. Demir, “Testing symmergent gravity through the shadow image and weak field photon deflection by a rotating black hole using the m87 and sgr. a results,” *The European Physical Journal C*, vol. 83, no. 3, p. 250, 2023.
- [89] İ. Çimdiker, D. Demir, and A. Övgün, “Black hole shadow in symmergent gravity,” *Physics of the Dark Universe*, vol. 34, p. 100900, 2021.
- [90] R. C. Pantig, L. Mastrototaro, G. Lambiase, and A. Övgün, “Shadow, lensing and neutrino propagation by dyonic modmax black holes,” *arXiv preprint arXiv:2208.06664*, 2022.
- [91] K. S. Virbhadra and G. F. Ellis, “Schwarzschild black hole lensing,” *Phys. Rev. D*, vol. 62, no. 8, p. 084003, 2000.
- [92] V. Perlick, “Theoretical gravitational lensing—beyond the weak-field small-angle approximation,” in *The Eleventh Marcel Grossmann Meeting: On Recent Developments in Theoretical and Experimental General Relativity, Gravitation and Relativistic Field Theories (In 3 Volumes)*, pp. 680–699, World Scientific, 2008.
- [93] S. Frittelli, T. P. Kling, and E. T. Newman, “Spacetime perspective of schwarzschild lensing,” *Phys. Rev. D*, vol. 61, no. 6, p. 064021, 2000.
- [94] V. Bozza, S. Capozziello, G. Iovane, and G. Scarpetta, “Strong field limit of black hole gravitational lensing,” *General Relativity and Gravitation*, vol. 33, pp. 1535–1548, 2001.
- [95] N. Tsukamoto, “Deflection angle in the strong deflection limit in a general asymptotically flat, static, spherically symmetric spacetime,” *Phys. Rev. D*, vol. 95, no. 6, p. 064035, 2017.
- [96] N. Tsukamoto, Y. Gong, *et al.*, “Retrolensing by a charged black hole,” *Phys. Rev. D*, vol. 95, no. 6, p. 064034, 2017.
- [97] E. F. Eiroa and D. F. Torres, “Strong field limit analysis of gravitational retrolensing,” *Phys. Rev. D*, vol. 69, no. 6, p. 063004, 2004.
- [98] E. F. Eiroa, G. E. Romero, and D. F. Torres, “Reissner-nordström black hole lensing,” *Physical Review D*, vol. 66, no. 2, p. 024010, 2002.
- [99] V. Bozza, F. De Luca, G. Scarpetta, and M. Sereno, “Analytic kerr black hole lensing for equatorial observers in the strong deflection limit,” *Phys. Rev. D*, vol. 72, no. 8, p. 083003, 2005.
- [100] S. E. Vazquez and E. P. Esteban, “Strong field gravitational lensing by a kerr black hole,” *arXiv preprint gr-qc/0308023*, 2003.
- [101] V. Bozza, “Quasiequatorial gravitational lensing by spinning black holes in the strong field limit,” *Physical Review D*, vol. 67, no. 10, p. 103006, 2003.
- [102] A. B. Aazami, C. R. Keeton, and A. Petters, “Lensing by kerr black holes. ii: Analytical study of quasi-equatorial lensing observables,” *J. Math. Phys.*, vol. 52, no. 10, 2011.
- [103] V. Bozza, F. De Luca, and G. Scarpetta, “Kerr black hole lensing for generic observers in the strong deflection limit,” *Phys. Rev. D*, vol. 74, no. 6, p. 063001, 2006.
- [104] V. Bozza and G. Scarpetta, “Strong deflection limit of black hole gravitational lensing with arbitrary source distances,” *Phys. Rev. D*, vol. 76, no. 8, p. 083008, 2007.
- [105] N. Tsukamoto, T. Harada, and K. Yajima, “Can we distinguish between black holes and wormholes by their einstein-ring systems?,” *Phys. Rev. D*, vol. 86, no. 10, p. 104062, 2012.
- [106] G. W. Gibbons and M. Vyska, “The application of weierstrass elliptic functions to schwarzschild null geodesics,” *Class. Quant. Grav.*, vol. 29, no. 6, p. 065016, 2012.
- [107] N. Tsukamoto, “Strong deflection limit analysis and gravitational lensing of an ellis wormhole,” *Phys. Rev. D*, vol. 94, no. 12, p. 124001, 2016.
- [108] N. Tsukamoto, “Retrolensing by a wormhole at deflection angles π and 3π ,” *Phys. Rev. D*, vol. 95, no. 8, p. 084021, 2017.
- [109] R. Shaikh, P. Banerjee, S. Paul, and T. Sarkar, “Strong gravitational lensing by wormholes,” *JCAP*, vol. 2019, no. 07, p. 028, 2019.
- [110] R. Shaikh and S. Kar, “Gravitational lensing by scalar-tensor wormholes and the energy conditions,” *Phys. Rev. D*, vol. 96, no. 4, p. 044037, 2017.
- [111] P. Aschieri, C. Blohmann, M. Dimitrijević, F. Meyer, P. Schupp, and J. Wess, “A gravity theory on noncommutative spaces,” *Classical and Quantum Gravity*, vol. 22, no. 17, p. 3511, 2005.
- [112] A. H. Chamseddine, “Deforming einstein’s gravity,” *Physics Letters B*, vol. 504, no. 1-2, pp. 33–37, 2001.
- [113] X. Calmet and A. Kobakhidze, “Second order noncommutative corrections to gravity,” *Physical Review D*, vol. 74, no. 4, p. 047702, 2006.
- [114] X. Calmet and A. Kobakhidze, “Noncommutative general relativity,” *Physical Review D*, vol. 72, no. 4, p. 045010, 2005.
- [115] A. Smailagic and E. Spallucci, “Feynman path integral on the non-commutative plane,” *Journal of Physics A: Mathematical and General*, vol. 36, no. 33, p. L467, 2003.
- [116] A. Smailagic and E. Spallucci, “Uv divergence-free qft on noncommutative plane,” *Journal of Physics A: Mathematical and General*, vol. 36, no. 39, p. L517, 2003.
- [117] A. Smailagic and E. Spallucci, “Lorentz invariance, unitarity and uv-finiteness of qft on noncommutative spacetime,” *Journal of Physics A: Mathematical and General*, vol. 37, no. 28, p. 7169, 2004.
- [118] P. Nicolini, A. Smailagic, and E. Spallucci, “Noncommutative geometry inspired schwarzschild black hole,” *Physics Letters*

- B*, vol. 632, no. 4, pp. 547–551, 2006.
- [119] J. Campos, M. Anacleto, F. Brito, and E. Passos, “Quasinormal modes and shadow of noncommutative black hole,” *Scientific Reports*, vol. 12, no. 1, p. 8516, 2022.
- [120] M. Bartlett and J. Moyal, “The exact transition probabilities of quantum-mechanical oscillators calculated by the phase-space method,” in *Mathematical Proceedings of the Cambridge Philosophical Society*, vol. 45, pp. 545–553, Cambridge University Press, 1949.
- [121] K. Nozari and S. H. Mehdipour, “Hawking radiation as quantum tunneling from a noncommutative schwarzschild black hole,” *Classical and Quantum Gravity*, vol. 25, no. 17, p. 175015, 2008.
- [122] C. W. Robson, L. Di Mauro Villari, and F. Biancalana, “Topological nature of the Hawking temperature of black holes,” *Phys. Rev. D*, vol. 99, no. 4, p. 044042, 2019.
- [123] A. Övgün and I. Sakalli, “Hawking Radiation via Gauss-Bonnet Theorem,” *Annals Phys.*, vol. 413, p. 168071, 2020.
- [124] Y.-P. Zhang, S.-W. Wei, and Y.-X. Liu, “Topological approach to derive the global Hawking temperature of (massive) BTZ black hole,” *Phys. Lett. B*, vol. 810, p. 135788, 2020.
- [125] A. Achúcarro and M. E. Ortiz, “Relating black holes in two-dimensions and three-dimensions,” *Phys. Rev. D*, vol. 48, pp. 3600–3605, 1993.
- [126] S.-W. Wei and Y.-X. Liu, “Observing the shadow of einstein-maxwell-dilaton-axion black hole,” *Journal of Cosmology and Astroparticle Physics*, vol. 2013, no. 11, p. 063, 2013.
- [127] U. Papnoi and F. Atamurotov, “Rotating charged black hole in 4d einstein–gauss–bonnet gravity: Photon motion and its shadow,” *Physics of the Dark Universe*, vol. 35, p. 100916, 2022.
- [128] B. E. Panah, K. Jafarzade, and S. Hendi, “Charged 4d einstein-gauss-bonnet-ads black holes: Shadow, energy emission, deflection angle and heat engine,” *Nuclear Physics B*, vol. 961, p. 115269, 2020.
- [129] S. Sau and J. W. Moffat, “Shadow of a regular black hole in scalar-tensor-vector gravity theory,” *Physical Review D*, vol. 107, no. 12, p. 124003, 2023.
- [130] S. Iyer and C. M. Will, “Black Hole Normal Modes: A WKB Approach. 1. Foundations and Application of a Higher Order WKB Analysis of Potential Barrier Scattering,” *Phys. Rev. D*, vol. 35, p. 3621, 1987.
- [131] S. Iyer, “BLACK HOLE NORMAL MODES: A WKB APPROACH. 2. SCHWARZSCHILD BLACK HOLES,” *Phys. Rev. D*, vol. 35, p. 3632, 1987.
- [132] R. A. Konoplya, “Quasinormal behavior of the d-dimensional Schwarzschild black hole and higher order WKB approach,” *Phys. Rev. D*, vol. 68, p. 024018, 2003.
- [133] J. Matyjasek and M. Opala, “Quasinormal modes of black holes. The improved semianalytic approach,” *Phys. Rev. D*, vol. 96, no. 2, p. 024011, 2017.
- [134] S.-W. Kim, “Gravitational perturbation of traversable wormhole,” *arXiv preprint gr-qc/0401007*, 2004.
- [135] B. F. Schutz and C. M. Will, “Black hole normal modes - A semianalytic approach,” *APJL*, vol. 291, pp. L33–L36, Apr. 1985.
- [136] R. A. Konoplya, “Quasinormal modes of the Schwarzschild black hole and higher order WKB approach,” *J. Phys. Stud.*, vol. 8, pp. 93–100, 2004.
- [137] V. Santos, R. V. Maluf, and C. A. S. Almeida, “Quasinormal frequencies of self-dual black holes,” *Phys. Rev. D*, vol. 93, no. 8, p. 084047, 2016.
- [138] R. A. Konoplya and A. Zhidenko, “Quasinormal modes of black holes: From astrophysics to string theory,” *Rev. Mod. Phys.*, vol. 83, pp. 793–836, 2011.
- [139] E. Berti, V. Cardoso, and A. O. Starinets, “Quasinormal modes of black holes and black branes,” *Class. Quant. Grav.*, vol. 26, p. 163001, 2009.
- [140] H. Chen, T. Sathiyaraj, H. Hassanabadi, Y. Yang, Z. W. Long, and F. Q. Tu, “Quasinormal modes of the EGUP-corrected Schwarzschild black hole,” *Indian Journal of Physics*, May 2023.
- [141] N. Heidari, H. Hassanabadi, A. A. Araújo Filho, J. Kriz, S. Zare, and P. J. Porfírio, “Gravitational signatures of a non-commutative stable black hole,” *Physics of the Dark Universe*, p. 101382, 2023.
- [142] N. Heidari, H. Hassanabadi, J. Kriz, *et al.*, “Exploring non-commutativity as a perturbation in the schwarzschild black hole: Quasinormal modes, scattering, and shadows,” *arXiv preprint arXiv:2308.03284*, 2023 – accepted for publication in The European Physical Journal C.
- [143] G. W. Gibbons and M. C. Werner, “Applications of the Gauss-Bonnet theorem to gravitational lensing,” *Class. Quant. Grav.*, vol. 25, p. 235009, 2008.
- [144] N. Tsukamoto, “Deflection angle in the strong deflection limit in a general asymptotically flat, static, spherically symmetric spacetime,” *Phys. Rev. D*, vol. 95, no. 6, p. 064035, 2017.
- [145] J. R. Nascimento, A. Y. Petrov, P. J. Porfírio, and A. R. Soares, “Gravitational lensing in black-bounce spacetimes,” *Phys. Rev. D*, vol. 102, no. 4, p. 044021, 2020.
- [146] A. A. Araújo Filho, J. R. Nascimento, A. Y. Petrov, and P. J. Porfírio, “Gravitational lensing by a lorentz-violating black hole,” *arXiv preprint arXiv:2404.04176*, 2024.
- [147] W. Hasse and V. Perlick, “Gravitational lensing in spherically symmetric static spacetimes with centrifugal force reversal,” *Gen. Rel. Grav.*, vol. 34, pp. 415–433, 2002.